4 Influence of the Crystal Structure Defects on Scintillation Properties

Abstract. This chapter discusses the influence of different crystal structure defects on the scintillation crystal conversion efficiency, energy transfer, luminescence yield and light collection, as well as on their radiation hardness. During the synthesis of crystalline media defects are inevitably produced and are classified according to their size and shape: point, linear and three-dimensional defects. Another type of defects are produced in the scintillators under ionizing radiation. Charged particles as light as electrons create charge defects in crystals. Heavier charged particles like protons, α-particles, hadrons and nuclear fragments loose much more energy when colliding with the lattice ions, resulting in relatively large damaged area of several crystallographic cells. The impact of these radiation induced defects on the radiation damage is presented, in particular on the scintillation efficiency and on crystal transparency. The dynamic of these effects is discussed in detail, for the damage building as well as for its recovery. The chapter concludes with practical considerations on how to improve scintillator radiation hardness.

The crystal scintillation properties are strongly related to their crystallographic structure. In spite of fact that the majority of scintillation crystals are isotropic for the propagation of light the scintillation efficiency depends on the other hand on the quality of the crystallographic structure and on the presence of defects. In fact all the components of the scintillation yield (conversion efficiency, transport, luminescence yield and light collection) are to some extent dependent on the structural quality of the lattice.

The conversion efficiency can vary as a function of the crystal alloying by replacement of a fraction of lattice ions by isovalent ions. It is also dependent on modifications of solid solutions which is one of the modern trends in research and development of new scintillators, for example LYSO and LuYAP.

The energy transfer is influenced by a wide range of structure-sensitive phenomena, for example, carrier capture in deep and shallow traps, color centers and other radiation-induced defect formation, chemical transformations of the activator with parasitic centers, relaxation of electronic excitations at point defects, etc.

The yield of luminescence depends also on the quality of the crystal. The selection of the optimum activator concentration and its homogeneous distribution in the crystal lattice are necessary to optimize this parameter.

Harmful impurities cause perturbations in the scintillation mechanism and are often related to the appearance of afterglow phenomena.

The light collection is extremely sensitive to the material transparency. The presence of absorbing and scattering centers in a host crystal, inhomogeneity of refractive index due to internal stresses, etc. are common sources of light losses.

The different causes of scintillation loss are schematically shown in Fig. 4.1. It is clear that all of them are directly or indirectly connected with imperfections of the crystal structure.

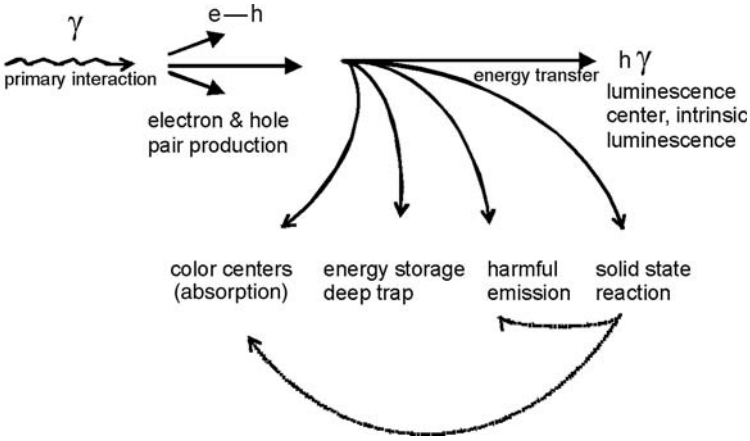

Fig. 4.1. A channel of scintillation loss

In most of the cases scintillators are based on single crystals which provide the best and most homogeneous conditions for the scintillation process: (i) minimization of parasitic defects, excitation and trap carriers, (ii) maximum purity of the material, (iii) optimum distribution of the activator, etc. More detailed information about single crystal growth, purity, and quality is given in Chap. 6.

4.1 Scintillation Media

In addition to single crystalline scintillators other solid inorganic materials are known and widely used. The role of the defects in such media is different from the single crystalline form.

- *Scintillation glasses.* These were the first choice for high energy physics in the mid 1960s. Li-based glasses are the cheapest commercially available solution for neutron detection [1]. A glass scintillator composed of Tb-doped gadolinium silicate glass is used in large area and fiber optic plate detectors

for industrial X-ray inspection systems [2]. Glasses are attractive media because of their relatively simple technology. On the other hand, the irregular lattice structure does not allow us to create efficient carrier transfer conditions and as a result all known glass scintillators have a relatively low light yield.

- *Polycrystalline scintillators.* Single crystal press forging is the way to increase the mechanical strength of materials. "Single-polycrystal" transformation is a typical procedure for material hardening. The easy to cleave crystals (such as alkali halides) can be forged or extruded at elevated temperatures for some applications, for example well logging that requires rugged scintillators [3]. Some time ago forging technique was efficiently developed for the large area scintillator design used for Anger (SPECT) camera [4]. It was found that the specific plastic deformation and the introduction of internal stresses did not suppress significantly the luminescence yield [5].
- *Scintillation powder.* This scintillation medium is typical for the screen development and applications. The low transfer of light between powder grains allows us to obtain a high spatial resolution in such screens. X-ray phosphor powders are extensively used in medical digital radiography. There are two main options for these materials: conventional intensifying screens and photo stimulated storage screens. Examples are LaOBr:Tm and Gd_2O_2:SiTb for X-ray intensifiers and BaFBr:Eu [6] based screens for storage applications. However, the problem of producing X-ray screens with a high scintillation efficiency is not really solved yet. Scintillation powder in itself is not a very convenient material for practical use. Therefore in the beginning of the 1980s a new technology was developed for the production of scintillators in the form of fine-dispersive particles distributed in an organic polymerized material matrix [7–10]. In particular, BaFCl:Eu and BaFBr:Eu powders in polyvinylnaphthalenetoluene matrix, alkali halides doped by Tl ions mixed with organic compounds of the benzene series [8], or organic siloxanes [11], etc. were proposed as the media for low energy X-ray detection. The organic material must have a refraction index as close as possible to the one of the powder. The advantage of such a method is the possibility of making detectors of any area, shape, and thickness. It may be used as a coating on practically all substrates. Such scintillators ensure a maximum light collection and a good matching to the light receiver.
- *Scintillation ceramics.* These types of scintillators have been developed and used for medical and industrial CT applications [12, 13]. Several compositions of such ceramics are shown in Table 4.1 with a relatively high yield, reasonable radiation hardness, and low afterglow in spite of the high concentration of structure defects. Typical ceramics have an average grain size of 30 μm and reach after isostatic pressing a relative density of more than 99.9% of the corresponding single crystal. These scintillators are usually slightly transparent or even translucent but the recent trend is to produce

more and more transparent ceramics by the introduction of nanotechnologies to produce very fine grain raw materials.

- *Scintillation films.* Epitaxial growth is the currently used method to obtain thin scintillation films. This is an efficient way for X-ray screen production. Practically all known bulk scintillation materials are also available in thin films.

Table 4.1. Comparison of some properties of single crystalline and ceramics scintillators

Material	X-ray attenuation coefficient (cm^{-1})		Emission λ (nm)	Relative light output (%)	Primary decay time (s)	After-glow (%)	Radiation damage (%)
	70 keV	500 keV					
CsI:Tl	34	0.49	550	100	1×10^{-6}	0.3	+13.5
$CdWO_4$	56	0.91	530	30	5×10^{-6}	0.02	−2.9
$Y_{1.34}Gd_{0.6}Eu_{0.06}O_3^f$	26	0.71	610	70	1×10^{-3}	<0.01	< -1.0
Gd_2O_2S:Pr,Ce,F	52	0.8	510	80	3×10^{-6}	<0.01	−3.0
$Gd_3Ga_5O_{12}$:Cr,Ce	32	0.7	730	40	14×10^{-5}	0.01	−0.3
$BaHfO_3$:Ce	64	0.95	400	15	25×10^{-9}	NA	NA

These examples illustrate the different criteria and influence of defects on the properties of scintillators. Nevertheless some basic principles have been progressively defined by experience in developing and optimizing scintillator production for large scale applications.

4.2 Defects in a Crystal

Traditionally the classification of crystal lattice defects is based on their size. Usually three kinds of defects—point, linear, and three-dimensional—are identified.

Point defects are ion vacancies and interstitials, impurity atoms or ions and their primary aggregates, radiation-induced defects like color centers. Such defects are characterized by quick internal stress relaxation with the distance from the point defect, and weak interaction with other defects.

Linear defects are dislocations with all possible configurations such as dislocation loops and/or dipoles and different dislocation substructures [14]. These defects, particularly when they appear in clusters, are the source of internal stresses.

Moving dislocations can discharge some isolated or aggregated point defects. Dislocations can also help charge transfer and color centers bleaching.

There are different kinds of three-dimensional defects which appear as macroscopic inclusions into the crystal lattice, for instance, foreign phases, voids, pores, and so on.

4.2.1 Internal Point Defects

There is always a certain concentration of internal point defects (anion and cation vacancies, some clusters of them) in a crystal in thermodynamic equilibrium. The equilibrium concentration of such defects is generally not high, about 10^{12} cm^{-3}, but their actual content may be much higher at room temperature. Plastic deformation of the material, internal stress relaxation, mechanical cutting, and sample treatment may introduce up to 10^{18} cm^{-3} vacancies. In specific cases crystal annealing at high temperatures can also increase the concentration of vacancies for example through the dissociation of electric dipoles [15, 16].

An increase of the concentration of vacancies leads to the formation of clusters of two, three, or even more vacancies [16]. Such defects do not influence the crystal transparency, although they can initiate the capture of carriers and energy storage mechanisms in the crystal.

In some crystals internal defects can induce absorption bands (especially in the UV range) which are likely to decrease the crystal transparency at the light emission wavelength. As an example we note that an increase of the absorption coefficient from $0.01\,\mathrm{cm}^{-1}$ up to $0.02\,\mathrm{cm}^{-1}$ in the scintillation light spectrum results in a decrease of the light output of the standard NaI(Tl) detector up to 30–40% and in a significant deterioration of the energy resolution.

4.2.2 Impurities

Impurities in crystals are far more diverse in comparison with internal point defects. It is related not only to the chemical elements diversity but also to the differences in electron shell structure types and valency and to the ability to create different kinds of dipoles and primary aggregates. Impurity ions with parameters close to some of the lattice ions can form solid solutions, i.e. states where they replace the matrix ions in some crystal lattice sites. This is particularly true for isovalent impurities with an ionic radius close to the one of some lattice ions. Heterovalent impurities can also be introduced in the crystal lattice but their excess (or deficit) charge must be compensated by other point defects. As a rule, heterovalent impurities form impurity-vacancy dipoles, and the electric neutrality of the lattice (charge compensation) is conditioned by their close association with the corresponding vacancy. In the recent years it has been stipulated that in some fluorides and complex

three- and four-component dielectrics the compensation may also occur by association with interstitials ions.

In general one can distinguish activating impurities (i.e. impurity influencing the scintillation process itself) and parasitic impurities that decrease scintillation efficiency.

4.2.3 Linear Defects

As a rule, only point defects are considered to influence the scintillator performance and their radiation hardness. Linear defects such as dislocations are assumed to have a small contribution to these effects. This approach is strictly speaking not correct. In the early 1980s the "deformation luminescence" phenomenon was discovered and described [17]. This effect embraces a range of phenomena during crystal deformation giving rise to the excitation of luminescence under the displacement of dislocations. In practice the internal stresses are not large enough to produce the displacement of dislocations. However, in the processes of crystal growth and during the mechanical treatment, deformation-induced effects may become quite large. There are other processes where the deformations influence the scintillator performances. A typical example is the press forging technique for the crystal hardening and density increase [4]. Crystal extrusion allows us to manufacture long length scintillators with practically the same scintillation performance as for single crystals grown by traditional methods. The first large samples of SPECT detectors were based on NaI(Tl) crystals deformed at high temperatures. Another example is the transformation of a single crystalline medium to a polycrystalline state. The progress of the forging technology allow us to obtain high material transparency, good scintillation performance (energy resolution), and good homogeneity of the polycrystalline bulk. As a matter of fact this technique of crystal preparation does not limit the crystal size. Figure 4.2 illustrates an example of a press forged NaI(Tl) crystal.

Different phenomena are observed in deformed crystals.

Moving dislocations cause the formation of numerous vacancies and vacancy complexes in crystals [15, 20]. The concentration of such defects may reach the level ($10^{18}\,\mathrm{cm}^{-3}$) which is comparable or even exceeds the concentration of impurities. Obviously, "deformation-induced" vacancies are in no way different from "normal" vacancies resulting from the thermodynamic equilibrium, but their concentration is by 5–6 orders of magnitude larger.

Post-deformation-induced luminescence is now a well-known phenomenon and it was described in [18] for the first time. Later, the same effect was studied for pure CsI in respect to fast UV scintillation optimization. It is possible to demonstrate the correlation between the luminescence yield and the excess of vacancies produced by plastic deformation. The vacancy concentration in this case grows with the increase of deformation (ε) as $\varepsilon^{2/3}$ [19]. In the luminescence spectra of such samples new bands at 460–480 nm appear as seen in Fig. 4.3. This new emission has a decay time of about 1–6 μm and is parasitic

Fig. 4.2. A NaI(Tl) large size slab after press forging

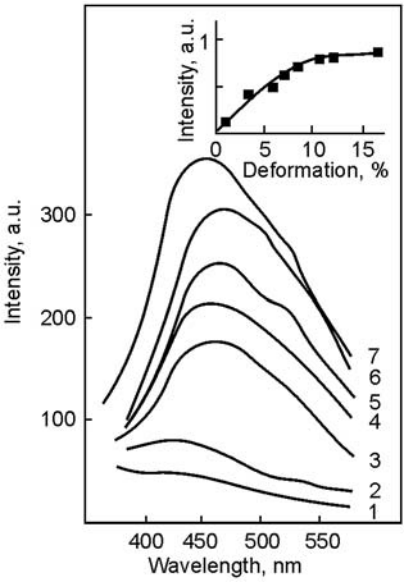

Fig. 4.3. Luminescence spectra of deformed CsI crystals: (*1*) no deformation, (*2*) 1%, (*4*) 3%, (*5*) 7%, (*6*) 8.5%, (*7*) 17%, (*3*) the same as (*7*) after 40 days of aging [20]

to the fast UV scintillation. With time the vacancy excess concentration is gradually relaxed through their diffusion and sink into dislocations and grain boundaries. However, the crystal does not reach the equilibrium concentration level (and, correspondingly, the fast/total ratio) even after dozens of days.

The deformation conditions (deformation rate and degree, the deformation temperature, crystallographic orientation of the sample, and so on) are

extremely important from the point of view of the introduction of vacancies, their stability, and evolution. In [15], for example, it was shown that point defects in alkali-halide crystals do not practically accumulate at temperatures higher than approximately 250 °C. They are actually being formed, but due to their high mobility, they sink to the dislocations.

The deformation sensitization of activated scintillators is an effect which is connected with dislocations in the crystal. Moving dislocations interact not only with each other but also with impurity defects (activator ions), which can be initially localized in the crystal lattice in a nonrandom way, especially for highly doped crystals where the distance between activator ions is not very big and they can easily interact with each other and form complex centers decreasing the luminescence efficiency. Moving dislocations can contribute to the activator homogenization. In [21] it was shown that in CsI(Tl) (7×10^{-2}% Tl) and CsI(Na) (8×10^{-3}% Na) the deformation did not change the luminescence spectra. But while increasing the CsI(Tl) deformation (0%, 2.8%, 6.6%), the ratio of the activator luminescence intensity was increasing as 1:2:2.3. A similar result was observed for CsI(Na) too for which the light output increased by a factor 1.5 after 3% deformation. This phenomenon was named "deformation sensitization" and can be applied not only to dielectrics but to semiconductor crystals also [22]. It illustrates the deformation engineering potential regarding the features of scintillation materials.

In spite of a long story of scintillators there are only a few scintillation materials where crystal defects were investigated in detail. Some of them are complex structure compounds. Oxides have in general a lower plasticity, higher hardness, and brittleness than halides. This is the reason for more precise studies of the influence of point defects on the scintillator performance. Lead tungstate (PWO) is a good example where characteristic defects have been studied by means of electron paramagnetic resonance (EPR) and thermo-stimulated luminescence (TSL).

PWO is very sensitive to the conditions of its synthesis. During the PWO crystal growth by the Czochralski method from stoichiometric raw material a dominant leakage of lead from the melt takes place, leading to the creation of cation vacancies V_c on the lead site in the host [23]. This is also confirmed for the crystals obtained by the modified Brigeman method [24].

Independently of the crystal growth technology, after an X-ray irradiation and the consequent filling of the traps created by point structure defects, only three characteristic electron centers can be observed in lead tungstate by EPR.

The shallowest of them occurs in all crystals since it is an intrinsic defect: an additional electron autolocalized at an anionic WO_4^{2-} complex via a Jan-Teller distortion creating a WO_4^{3-} polaronic center [25–27]. This trap is emptied near 50 K with an activation energy of 50 meV. The electrons released recombine radiatively or are caught by deeper traps.

The second one is a Pb^{1+}-V_0 center which is stable in the crystal up to 175 K [28, 29]. It is not excluded that instead of a Pb^{2+} ion another one (impurity related) may create such a center near an anion vacancy, but what is important is that an electron is trapped by a heterovalent cation in the vicinity of an oxygen vacancy. This center is clearly detected by a relatively large deviation of the g factor of all such magnetically nonequivalent species from g_e. This center is photoionized by IR light with a threshold of 0.9 eV.

The third one is a WO_4^{3-} electron center which is created on the basis of a regular tungstate anionic complex disturbed by a nearby rare-earth (RE) trivalent impurity ion such as La, Lu, or Y [26]. It decays near 97 K. Careful partial annealing experiments showed that the rate of decrease of the EPR intensity of WO_4^{3-}-La coincides with the TSL emission in this temperature region [28,29]. In addition, the doping of the crystal with stable trivalent RE ions such as La, Lu, Gd, and Y with concentrations of some tens of ppm redistributes electron trapping centers, reducing the number of deep ones [30,31]. Such ions localized at Pb sites introduce in the crystal an extra positive uncompensated charge and will thus compete with the creation of V_0 vacancies. In addition the doping ions introduced in a non perfectly stoichiometric crystal (due to PbO evaporation) occupy empty lead sites in the lattice and so suppress the superstructure fraction with its distorted tetrahedra in the crystal. Another way to compensate the cation vacancies is the creation of the 2RE-V_c centers during the doping. However, the small concentration of cation vacancies and compensating centers (typically less than 100 ppm) and their casual distributions in the melt and in the resulting crystal make the probability of creating such associations rather small.

Other intrinsic defects based on cation or anion vacancies with paramagnetic ground state, which are typical of other tungstate crystals, have never been detected in PWO crystals. This indicates that centers such as isolated F^+ (anion vacancy V_0+ e) and O^- have either no energy levels in the forbidden band or are delocalized in the conduction and valence bands. Therefore the only candidates for metastable color centers in PWO crystals under irradiation are cation vacancies capturing two holes of the type $O^-V_cO^-$ and oxygen vacancies simple or complex centers capturing even amounts of electrons.

In crystals with RE doping a second trap center is detected through TSL only with an activation energy of 130 meV. This center is not paramagnetic and is probably a RE-$(WO_4)^{4-}$ center. This is in agreement with the fact that RE-doped PWO crystals show a larger TSL intensity around 100 K as compared to undoped ones. An electron release from the 130 meV traps causes the simultaneous production of lower electron centers by retrapping, as well as through the creation of RE-$(WO_4)^{3-}$ giving an increase of TSL intensity in that resgion.

The deepest electron trap center is a Frenkel-type defect which occurs in the crystal as a result of the displacement of an oxygen ion into an intersite

position. The V_0 vacancy created by the Frenkel defect can also trap electrons giving a center such as $(WO_3)^{2-}$. Such a center appears at irradiation, is stable at room temperature, and shows absorption spectra close to the WO_3 center near the Frenkel defect. Frenkel defect produces an optical absorption band at 360 nm which is converted under ionizing radiation in an absorption band with a maximum near 410 nm. The defects associates and their trapping properties have been discussed in [23, 32].

Each type of defects can potentially influence the scintillation performance. Due to the disposition of electronic centers near the bottom of the conduction band it seems possible to distinguish the influence of each category of defects on the crystal scintillation properties. In spite of a fast exchange of electrons between shallow polaronic and RE distorted regular centers with the conduction band which contribute therefore to the scintillation, there is also a flow of electrons to the deep traps. At high WO_4^{2-}-RE centers, concentration in the crystal this outflow becomes so important that it produces a visible decrease of the crystal light yield. It appears therefore that the strong radiation hardness requirement for the PWO crystals imposes the doping with trivalent rare-earth ions which reduce the light yield of the crystal. The only possibility of meeting both radiation hardness and higher light yield would be to reach a much better structural quality of the crystal than is presently technically possible.

4.3 Change of the Optical and Luminescence Properties by Crystal Defects

4.3.1 Scintillation Light Absorption by Crystal Defects

Absorption bands as well as internal nonuniformities, for example scattered inclusions, gas bubbles, and voids, influence the light collection and contribute to light losses by scattering and absorption. This is particularly important for long scintillators as well as for IAD applications. This is why the study of the optical absorption spectrum in the scintillation emission range is a very important tool to probe the intrinsic quality of the crystal.

The most essential contribution to optical absorption is related to internal point defects, impurities, and radiation-induced point defects.

BaF_2 scintillator is one of the most illustrative examples to demonstrate the influence of impurities on optical and luminescent properties of a crystal. The major drawback of BaF_2 resulting from the emission in the deep UV range is to a great extent compensated by its ultrafast decay time. This behavior corresponds to a very specific mode of scintillation, the so-called cross-luminescence which was then discovered in several other materials (see Chap. 2).

For such materials it is necessary to achieve a very high transparency of the material in the UV range. The main problem is that alkali earth fluorides

are easily contaminated by oxygen and hydroxyl ions which are at the origin of strong absorption bands in the UV range. A theoretical study of the charge state stability and electronic structure of O^0, O^-, and O^{2-} centers in BaF_2 [33] allowed us to identify a large number of transitions from 2p to 3s and 5s states. In [34] Hartree–Fock–Slatter local density discrete variation cluster calculations were made to obtain the energy levels of H_s^-, O_s^-, and O_s^{2-} ions in BaF_2 crystals. Table 4.2 summarizes the possible optical absorption bands in the VUV and UV ranges.

Table 4.2. Calculated optical absorption band of H_s^-, O_s^--, and O_s^{2-}-doped BaF_2 [34]

Impurities	$\lambda_{abs.}$ (nm)	[eV]	Cross transitions
H_S^-	209	[5.9]	$H^-(1s) \rightarrow H^-$ (2s)
O_S^-	230	[5.4]	F^- (2p) $\rightarrow O^-$(2p,3p)
	175	[7.2]	F^- (2p) $\rightarrow$ O−(3p)
	170≈175	[7.0≈7.2]	O^- (2p) $\rightarrow Ba^2$+(5d)
O_S^{2-}	292	[4.2]	F^- (2p) $\rightarrow O^{2-}$ (3p)
	200	[6.2]	O^{2-}−(2p) $\rightarrow Ba^2$+(6s)
	130	[9.5]	O^{2-} (2p) $\rightarrow Ba^2$+(5d)

As far as O^- and O^{2-} ions are concerned, the absorption bands are mainly the result of cross transitions between oxygen ions and Ba^{2+} or F^- ions which significantly contribute to absorption around 200–240 nm.

The UV absorption spectrum of BaF_2 samples shows a strong absorption peak in hydrolyzed crystals as seen in Fig. 4.4 [34] which overlaps the fast emission band.

These problems are essentially caused by the presence of oxygen and hydroxyl ions in the material, but in an indirect way [35]. A good example is given by NaI(TI) crystals grown from melt with different hydrolysis levels or in an atmosphere reach in I_2.

The following reaction takes place at high temperatures [36]:

$$2NaI + H_2O + 1/2O_2 \rightarrow 2NaOH + I_2$$

It releases I_2 and NaOH accumulates in the melt. On the other hand, in iodide reach melt of alkali metals the metathesis decomposition reactions with oxygen predominate over hydrolytic reactions:

$$4NaI + O_2 \rightarrow 2Na_2O + 2I_2$$
$$2NaI + O_2 \rightarrow Na_2O_2 + I_2$$
$$NaI + O_2 \rightarrow NaO_2 + 1/2I_2$$
$$4NaI + 1/4O_2 + 1/2CO_2 \rightarrow 1/2Na_2CO_3 + 1/2I_2$$

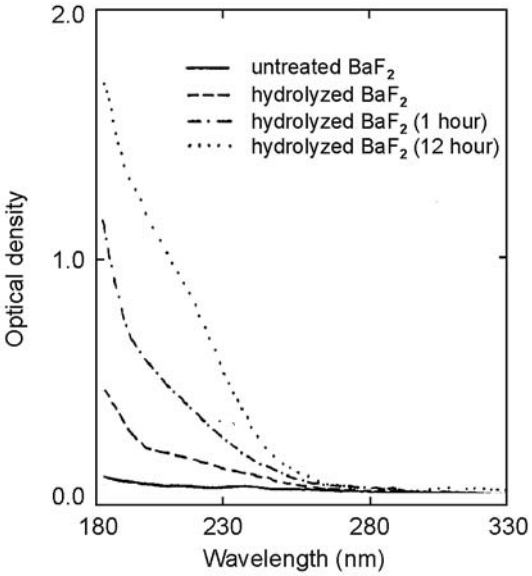

Fig. 4.4. Absorption spectrums for different hydrolyzed BaF_2 [34]

In the case of an excess of I_2 in the atmosphere there is also an increasing probability of generating poly-alkali I_3^- synthesis in NaI crystals [36, 37]. As a result of the accumulation of iodine in the crystal absorption bands appear which overlap with the activator's luminescent spectrum as seen in Fig. 4.5. These specific bands at 340–360, 380, 420, 470, and 520 nm are created by optical transitions between molecular states of I_2^0 molecules and more generally I_n ($n \geq 2$) of different structures and orientations. They are observed in several iodine-loaded solutions and matrixes [38] as well as in irradiated alkali-iodide crystals [39].

The negative influence of the intrinsic absorption in the range of scintillation is clearly seen in the deterioration of the NaI(Tl) crystal performances as shown in Fig. 4.6.

The presence of various impurities having absorption bands in the UV range also affects the transparency of a material in the range of scintillation emission. A typical example is Pb ions in BaF_2. The Pb^{2+} absorption peak efficiently absorbs the fast scintillation and is a critical issue for BaF_2 scintillator development. The data on the role of oxygen containing impurities and polyvalent anions on the detector scintillation efficiency are given in [40].

The negative influence of too high oxidization level in oxide crystals on their transmission spectrum is a well-known phenomenon. This is the reason for yellowish color of not well-optimized tungstate and molibdate crystals. In fact, two wide absorption bands with maxima near 370 and 420 nm cause the crystal's yellowish coloration [41, 42]. The origin of the long wavelength band

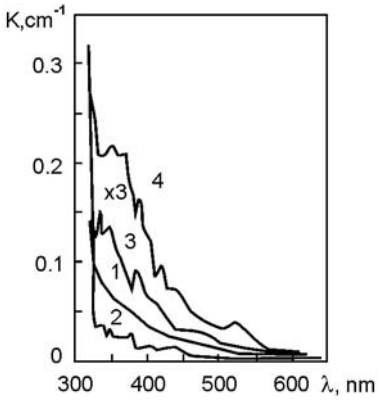

Fig. 4.5. Absorption spectra of NaI(TI) crystals, grown in melt hydrolysis conditions; (*1*) before annealing; (*2*) after annealing at 550°C; (*3*) spectrum 2 subtracted from spectrum 1, note the factor ×3 in scale; (*4*) NaI-I_2 crystal

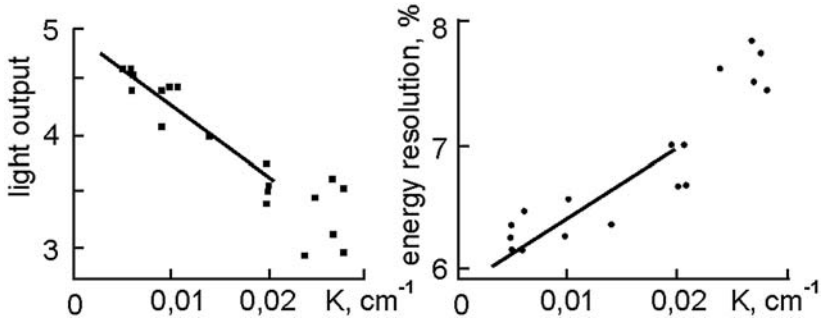

Fig. 4.6. Dependence of light output C (**a**) and energy resolution R (**b**) for NaI(TI) standard detectors

has been understood from the analysis of the electron density distribution in Bi-doped crystals [23, 43]. This band is related to a charge transfer transition in a localized gap state about 1 eV below the bottom of the conducting band. The same localized gap state is created by trivalent lead ions. Crystals grown in air usually show the 420-nm absorption band; however, this band is strongly suppressed in crystals grown in a neutral gas atmosphere or doped with trivalent RE. Moreover, the 420-nm band intensity increases when annealing in air at temperatures close to the crystal's melting point but it disappears under a long vacuum annealing followed by a fast temperature decrease, especially in Bi-doped crystals. However, the yellow color of Bi-doped crystals may be easily recovered just by short, about 5 h, annealing at 950 K in air. The diffusion of oxygen during the annealing is unlikely to explain such changes. One can state that both trivalent lead and bismuth impurity ions provoke the yellowish coloring of the crystal, although the former

seems to be dominant. The same absorption band is observed in lead molybdate as noted in [42] which can be easily predicted from the similarity of the electronic band structures of lead tungstate and molybdate.

4.3.2 Harmful Luminescence and Afterglow

Any luminescence with a decay time much longer than the main scintillation decay time can be defined as afterglow. As was discussed in Chap. 3, this phenomenon is important for different applications and in particular very critical for medical CT devices.

In practice, present technologies for the synthesis and single crystal growth do not allow us to reach an ideal purity and the level of residual parasitic impurities remains the essential limitation of the scintillation efficiency. The efficiency losses are connected with either carrier capture by various traps or energy storing sites. Consider the example of a pure CsI scintillator for which several models have been developed. This material is a unique example of intrinsic luminescence in the alkali-halide scintillators family [46] which found several applications because of its fast scintillation [44, 45]. Figure 4.7 shows its scintillation kinetics and time-resolved scintillation luminescence spectra.

Besides the fast 10-ns scintillation component related to the luminescence peak at 300 nm other emission bands are also observed. They are connected to other slowly decaying centers. In particular, the emission caused by the presence of oxygen ions in the crystal has been identified. These emissions in the green range have a decay time of several microseconds which is typical for ions such as O_2^-. Moreover under irradiation and/or temperature treatment reactions easily occur from O^{2-} ions to O_2^-. All these centers introduce additional harmful luminescence, quench the fast emission and cause afterglow to scintillation. The methods for preventing harmful luminescence and afterglow are generally related to the crystal growth technology. They are (i) preliminary purification of raw material, (ii) additional melt purification, and (iii) attempts to reach the best structure performance.

In activated scintillators one of the mechanisms at the origin of high afterglow level is related to the formation of complex activator luminescence centers. In CsI(Tl), for example, the radiation-induced spectrum shows contributions from Tl_2^0 and Tl^{2+} activator centers. Such centers are formed under UV irradiation. Their combination with F-centers is responsible for afterglow. To prevent the formation of such centers and decrease the amount of afterglow such crystals need to be stored in the dark.

The stability of such centers is not high and dissociation temperatures for Tl_2^0 and Tl^{2+} reach 70°C and 140 °C, respectively. Consequently, low-temperature (130–140°C) annealing of the crystals is also a way to lower the afterglow level and to increase the radioluminescence output by 40–50%.

However, there are examples of the positive role of some doping ions for the scintillation yield of the fast component related to cross-luminescent

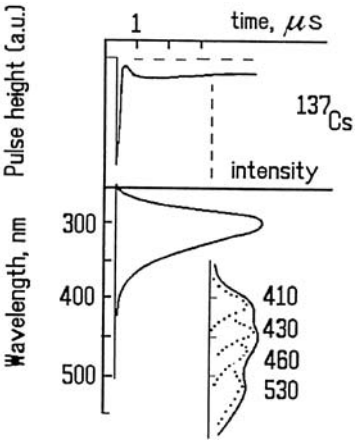

Fig. 4.7. Scintillation kinetics and time-resolved scintillation luminescence spectra of pure CsI scintillator [47]

scintillators, such as BaF_2. The ultrafast core valence luminescence (about 1 ns) in the crystals is accompanied by slow exciton luminescence (600 ns). Improvement of such kinds of scintillators requires quenching this excitonic luminescence. It was shown that different dopings of BaF_2 such as La, Y, Cd allow us to efficiently suppress the exciton luminescence [48].

The precipitation techniques used to synthesize transparent ceramic scintillators is a good approach for obtaining a homogeneous distribution of doping of ions used to reduce the afterglow. Afterglow in $(Y,Gb)_2O_3$:Eu scintillators can be significantly reduced by the addition of heterovalent Pr^{3+} or Tb^{3+} ions to the lattice [49]. The Pr^{3+} and Tb^{3+} additives readily trap holes to form Pr^{4+} and Tb^{4+} which compete with the intrinsic traps responsible for afterglow. This energy trapped on the Pr or Tb sites decays nonradiatively in the presence of Eu ion [50], so the afterglow emission is reduced. These techniques have been used to reduce afterglow in rare-earth oxides [51], oxysulfides [51, 52], and $Gd_3Ga_5O_{12}$:Cr,Ce [53] ceramic scintillators.

4.3.3 Low Background Problem

The influence of parasitic impurities on the background counting rate of scintillators is also an important aspect of the registration efficiency of scintillation materials for several applications. Some isotopes present in the host material are radioactive. There are lots of such intrinsic or extrinsic "radiative" elements, such as K, Cs, and Rb isotopes in halide scintillators or ^{176}Lu in all lutetium-based scintillators. This phenomenon can introduce nonnegligible counting rates for some applications. This is for example one major drawback of LSO for low-energy single photon emission computed tomography (SPECT) imaging as well as for low background applications. Lutetium

has a naturally occurring stable ^{176}Lu isotope that has a very long half-life, 10^{10} years. The abundance of this isotope is approximately 2.76% and it produces a beta decay resulting in several gammas in the range of approximately 100 keV to 700 keV. In a 20% energy window centered at 140 keV the count rate in a 4 mm by 4 mm by 10 mm pixel is approximately 2 counts s^{-1}. This is definitely an unacceptable background for a gamma camera application. It is much less a problem for a PET because of its working mode in coincidence.

4.4 Radiation Damage of Scintillators and Radiation Hardness Improvement

Scintillators as ionizing radiation sensors are naturally subject to radiation influence. Therefore the stability of their parameters under ionizing radiation is mandatory.

From a pragmatic point of view the question of scintillator radiation hardness is reduced to the estimation of the detector scintillation efficiency change when exposed to different kinds of radiation. The practical criterion of the scintillator resistance to radiation is the value of the scintillator efficiency losses under radiation, i.e. the reduction of its light yield. This criterion does not have an unambiguous interpretation as the level of radiation damage depends not only on the type of radiation but also on the dose, dose rate, and recovery (aging) conditions (such as optical bleaching, storage temperature, and exploitation). These aspects appear to be important in the definition of the criteria because they correspond to the working conditions of the detector in general. This is why the study of radiation damage in different scintillators is at the origin of a large multidisciplinary R&D effort carried out in many scientific laboratories worldwide.

From the physical point of view the problem is to study the deterioration mechanisms of the material optical transparency and of the luminescence yield.

The crystal transparency usually drops as a result of the formation of color centers under irradiation. This process obviously affects the light transport efficiency from the point of emission to the photodetector.

The luminescence yield can also be modified if the luminescence centers are subject to transformations under irradiation. Fortunately, the scintillation mechanism is very stable in many crystals, for example, in self-activated scintillation crystals such as $Bi_3Ge_4O_{12}$ and $PbWO_4$, where the oxy-anion complexes from the matrix are the luminescent centers. For these crystals the radiation damage is only related to the optical transmission damage through the formation of color centers. In activated scintillators (NaI(Tl), CsI(Tl), LSO:Ce, GSO:Ce, $LaBr_3$:Ce, and others) both the scintillation efficiency and the crystal transparency can be potentially damaged under irradiation.

The possible impact of the radiation damage is very dependent on the application. If we consider for example the criteria and measurements of the

radiation damage for application of medical imaging (CT) and HEP detectors, they are clearly different. If, in the first case, instability is defined as a change of the functional parameters by a few percents only, in the second case, where the radiation dose is by 5–6 orders of magnitude greater, the light yield deterioration can reach several tens of percents. Depending on whether we consider low or high doses and dose rates the damage mechanisms can be different.

One of the most demanding applications in terms of radiation hardness is high energy physics (HEP). This problem has encouraged large scale R&D efforts on scintillator radiation damage studies.

Since the last decade the development of HEP projects has been based on the development of BaF_2 scintillators for the Superconducting Super Collider (SSC) project [54] in the United States, as well as CeF_3 and PWO crystals for the Large Hadron Cllider (LHC) at CERN in Europe [55]. One of the most critical requirements for these scintillators was to reach a low level of radiation damage [56]. The other example of recent years' developments concerns radiation hard CsI(Tl) scintillator for medium energy physics projects such as BELLE [57] and BaBar [58]. The same basic problems and physical mechanisms have been seen in both classes of materials. The effect of radiation damage results from a combination of two components. The first is connected with structure defects preexisting in the crystal, and the second is conditioned by the defects being produced in the crystal by the interaction with the radiation.

4.4.1 Radiation Defects in Dielectrics

Charged particles even as light as electrons create defects in crystals. About 1 MeV electrons are able to transmit a kinetic energy of the order of 50 eV to an ion. Heavier charged particles such as protons, α-particles, hadrons, and nuclear fragments lose much more energy when collide with the lattice ions. For such interactions with heavy particles, even with a modest energy of about 1 MeV, a relatively large area of several crystallographic cells can be damaged.

Neutron bombardment, either slow or fast, causes the greatest damage to the crystal structure. Slow neutrons have in general a large capture cross section by the different atoms of the crystal cell. When this happens a considerable energy is released, which creates important defects in the crystal. A neutron with an energy of 1 MeV colliding with an oxygen atom transfers an energy of $\sim$40 keV. Consequently a strong neutron bombardment causes deep changes in the crystalline structure of inorganic compounds.

The results of all these interactions are radiation-induced modifications of the crystalline dielectric structure. They are of the same type for various crystalline compounds and different types of ionizing radiation with the only difference that the doses and the dose rates necessary to produce the same effect are substantially different from material to material. Such structure

modifications observed under irradiation can be divided into several groups [59].

The first group consists of microscopic structure changes for which the main structure parameters and particularly the spatial symmetry group do not change. This is by far the most frequent case where the most important parameter is the concentration of initial defects in the crystal inducing the capture of free carriers by vacancies and their recombinations, defects aggregations, sink into dislocations, grain boundary, and crystal surface effects. This concerns the majority of cases where the irradiation rate level is not too high (this is even true up to the dose rates expected in the LHC). There is a rapid relaxation of the lattice and the damage is limited to some electronic structure reconfigurations in the vicinity of preexisting defects in the crystal.

Radiation defects are specific for every kind of ionizing radiation and are determined by the structural configuration of the lattice.

The macroscopic observed effects in the crystals, such as optical transmission, conductivity, and thermo-luminescence properties, result from the integration on a large volume of microscopic structure modifications.

The second group of structure changes consists of modifications of the configuration of the nearest surrounding atom. In a way, this corresponds to the formation of a kind of superstructure associated with the preexisting defects. This situation appears when the defect concentration becomes comparable to the content of some of matrix ions or atoms, i.e. concentrations of the order of 10^{18}–10^{20} cm^{-3}.

Deeper structural changes are generally related to extrinsic element inclusions and substantial deviations from stoichiometry. This corresponds to the radiolysis stage. Such changes are typical, for example, for neutron irradiation with integral fluence of $\sim 10^{20}$ neutrons or more. Such changes have been observed in many compounds under neutrons, electrons, and γ-irradiation [60, 61]. At this level of irradiation the scintillation mechanisms are strongly degraded. At a relatively low dose rate ionizing radiation induces charge transfer to some matrix ions and vacancies preexisting in the crystal before irradiation.

In ionic crystals, containing anions and cations, five possible simple point defects of the crystalline structure have been observed: anion vacancy V_a, cation vacancy V_c, cation replacement by impurity ions, extrinsic atoms in intersite positions, and Frenkel-type defects (anions and cations in interstitial sites).

In halide crystals the electron captured by anion vacancy forms F-center ($V_a + e^-$). In oxide compounds the oxygen vacancies, depending upon the energy level of the corresponding electron traps in the forbidden band, capture one or two electrons, which are in excess in the conduction band after irradiation, with the formation of $F^+(V_a + e^-)$ and $F(V_a+2e^-)$ electron centers. Cation vacancies, in contrast, capture excess holes from the valence band, forming one- and two-hole centers. Heterovalent matrix and impurity

ions undergo modification of their electronic configuration under the influence of ionizing radiation. Frenkel defects, as a result of the displacement of an anion or cation, behave as electron or hole centers, respectively.

In oxide crystals interstitial oxygen causes a distortion of the nearest oxygen polyhedra, creating additional shallow electron traps. Once they have trapped electrons or holes (it is said that they are recharged defects) the defects are in a stable or metastable state. In many cases electron and hole centers (especially Frenkel-type defects) are metastable at room temperature and their relaxation is characterized by a complex decay time curve. To a certain extent, all the color centers are metastable because there is always a temperature at which the annihilation of electron and hole centers takes place, which leads to the recovery of the lattice to its original state.

The main peculiarity of many recharged defects is their ability to absorb light, i.e. to create absorption bands in the transparency window of the scintillator. For this reason these defects are called color centers [62]. The intensity of the absorption depends on the concentration of the color centers as well as on their type, through the cross section of photons to create electronic transitions. Naturally, the effect of induced absorption for metastable centers is temporary. Such centers generally exhibit a natural recovery of the transparency of the crystal with a temperature-dependent kinetics.

The formation and accumulation of color centers in ionic crystals is a multistep process [63, 64]. The first stage of accumulation is connected with the carrier capture by preexisting defects. In this case the energy of formation of color centers is usually small. It is obvious that the kinetics of the accumulation of color centers at this stage depends on the quality of the initial structure and on the purity of the single crystal.

With irradiation doses of the order of 0.1–1.0 Mrad the second stage of crystal coloring takes place, where the accumulation of color centers is caused by their formation and stabilization at regular sites of the lattice [64]. This stage of the accumulation of color centers also depends on the quality of the crystal structure. For most of the HEP modern experiments the requirement for a good stability of scintillator performances is for doses in the 1–10 Mrad range.

At the third stage an active aggregation of color centers and the formation of inclusions from crystal components start to take place [65]. The aggregation of such kind of defects can lead to the formation of colloid metal particles in a crystal. The sizes of the particles are such that their absorption bands can also be within the visible range of wavelengths and absorb scintillation photons [66].

4.4.2 Radiation Stimulated Losses of Scintillator Transparency

As a result of the previous consideration it appears clearly that for the majority of practical situations the damage is essentiality the result of an increased

absorption in the crystal. This mechanism is extremely important and therefore let us consider it in more details.

4.4.2.1 Color Centers and Transparency Losses

As a typical example let us consider CsI(Tl) crystals. CsI(Tl) radiation damage has been discussed by many authors [67–71]. Test results for long CsI(Tl) scintillators were described in [70, 72] but the physical nature of scintillation efficiency decrease has not been considered.

Figure 4.8 shows an optical absorption spectrum for CsI crystals containing various color centers. F-centers formed by electrolytic electron coloration create an absorption band with a maximum at 780-nm. The 780-nm band absorbs only a small portion of the light from the 550-nm emission band. Three experiments were performed to study the absorption of hole color centers. Induced absorption spectra were measured for an aqueous solution of Csl + I_2 (curve 1), CsI crystals additively colored in iodine vapors (curve 2), and the same crystals subject to electrolytic hole coloration (curve 3). In all cases absorption bands with 280 and 340 nm maxima, corresponding to

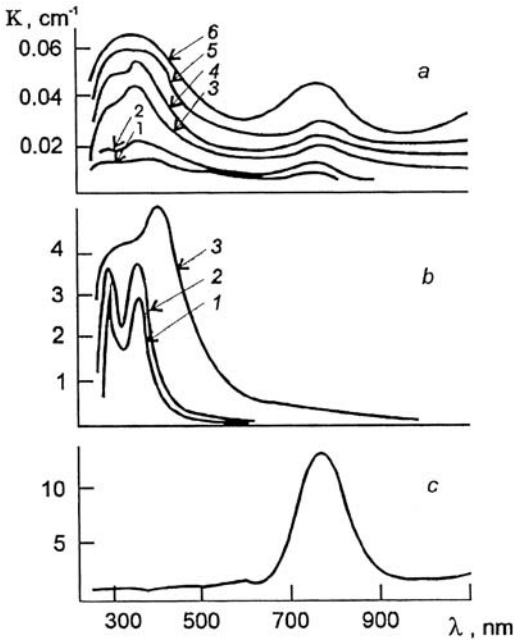

Fig. 4.8. Induced absorption spectra relative to an uncolored CsI sample. **a** γ-irradiation (^{60}Co, 0.2 MRh^{-1}) with doses (MR): 0.01 (*1*); 0.06 (*2*); 0.12 (*3*); 0.69 (*4*); 2.2 (*5*)); 7.2 (*6*). **b** Hole coloration: I_2 dissolved in CsI aqueous solution (*1*); additively colored crystal (*2*); electrolytically (holes) colored crystal (*3*). **c** Elecrolytically (electrons) colored crystal

the so-called V_2 and V_3 color centers [73–75], were observed. In γ-irradiated samples, color centers of both electron and hole types are formed (Fig. 4.8a).

The absorption of hole centers is situated in the wavelength range of excitation of Tl ions. As a matter of fact the absorption of hole centers reduces the energy transfer to the luminescence centers. A wide band of electron color centers overlaps a part of the CsI(Tl) luminescence band so that part of the scintillation light is reabsorbed inducing a reduction of the light collection efficiency (see Chap. 6) and of the scintillator overall light yield.

In the case of formation of stable color centers in a crystal the absorption of scintillation photons is proportional to the reduction of crystal transparency convoluted to the emission spectrum. In this case the efficiency losses are easily calculated by the classic methods of light collection estimation [76, 77].

In the general case, however, radiation-induced variations of the light yield are to be attributed not only to the degradation of the crystal transmission but also to possible variations in the conversion efficiency. The calculated curves of the light yield change along the scintillator length for different induced absorption and conversion efficiency are shown in Fig. 4.9 [72].

While increasing the absorption coefficient at the emission wavelength, the light output decreases. In this case it is not the number of scintillation photons in the crystal which decreases but the share of these photons yielding out of the crystal. It is also important to notice that the number of photons collected at the end of a long crystal becomes sensitive to the position where the scintillation took place, and as it moves from the detector exit window, the value of the light yield constantly decreases.

When simulating the efficiency losses due to the transparency degradation in an irradiated crystal, one should take into account that the distribution

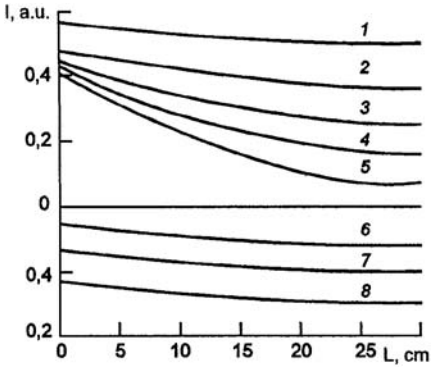

Fig. 4.9. Light output versus longitudinal coordinate for various values of light absorption coefficient k (cm^{-1}) and conversion efficiency η (arbitrary units): (*1*) $k = 0.01$; (*2*) $k = 0.02$; (*3*) $k = 0.03$; (*4*) $k = 0.04$; (*5*) $k = 0.06$; (*6*) $k = 0.01$, $\eta = 1$; (*7*) $k = 0.01$, $\eta = 0.85$; (*8*) $k = 0.01$, $\eta = 0.68$

of color centers with the crystal is simply related to both the distribution of defects in the crystal structure and the distribution of the absorbed energy (Buger's formula) which is in general not homogeneous. For medium energy particles (several MeV) the radiation dose close to the entrance surface is by the orders of magnitude higher than on the opposite face of the detector. At higher energies (GeV) the peak of the energy release is at several radiation lengths (5 to 7) from the entrance window. Correspondingly the crystal coloring (i.e. distribution of color centers) is not homogeneous. This effect must be taken into account both while testing samples and simulating the light collection in a scintillator. This is especially important for high-energy physics. In long-length crystals, usually used in electromagnetic calorimeters, radiation losses due to reabsorption of scintillations by color centers are the dominant effect because of the long path length of light rays related to the length of the crystal and to the large number of light reflections on side surfaces of the scintillator block.

4.4.2.2 Metastable Color Centers

It must be realized that the phenomenological behavior of a scintillator exposed to radiation depends not only on the situation of stable defects but is also very much influenced by metastable color centers, particularly in a range of dose rate corresponding to the kinetics of these defects. Moreover, there are also short lifetime color centers created simultaneously with the excitation of the emission centers. Such centers are connected with very shallow traps and can absorb the scintillations light, i.e. cause short lifetime (also called transient) induced absorption bands.

Let us consider a simple model where ionizing radiation produces at the same time excited luminescence centers and color centers with concentrations $n^i(t)$, $n^c(t)$ decaying with time constants τ^i and τ^c, respectively. Assuming these concentrations of emission centers and color centers to be small enough to neglect correlation effects between them, we can consider that color centers disappear as a result of the recombination of electron and hole centers, as well as of their photoionization under the absorption of scintillation photons with cross section σ. Moreover, the length 1 of the scintillator is such that $1/c \ll \tau^d$, τ^c, where c is the speed of light. Let's define f as the total number of photons detected by the photodetector with a response time $\tau^d \ll \tau^c$ and a detection efficiency equal to 1. For simplicity the light collection problems and spectral distribution of the light are not considered here. Thus the system evolution is described by the kinetic equations [78]:

$$\begin{aligned} \frac{\mathrm{d}n^i}{\mathrm{d}t} &= -\frac{1}{\tau^i} n^i \,, \\ \frac{\mathrm{d}n^c}{\mathrm{d}t} &= -\frac{1}{\tau^c} n^c - c\sigma n^c f \,, \\ \frac{\mathrm{d}f^i}{\mathrm{d}t} &= \frac{1}{\tau^i} n^i - c\sigma n^c f - \frac{1}{\tau^d} f \,. \end{aligned} \tag{4.1}$$

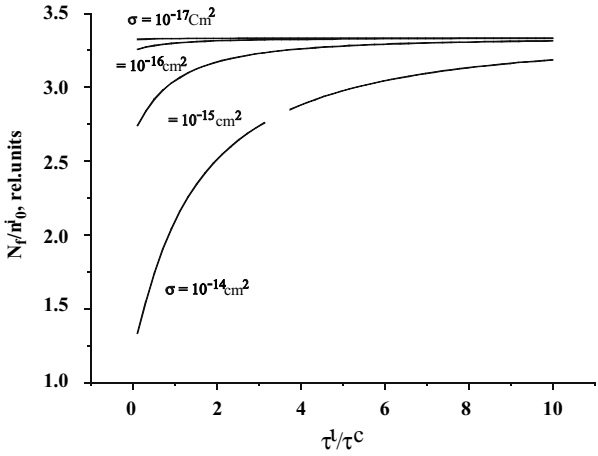

Fig. 4.10. N_f dependence upon the relation τ^i/τ^c for different cross sections of scintillation light absorption by short lifetime color centers

The scintillator response, which is proportional to the number of photons, to be detected by the photodetector, is $N_f = \int_0^\infty f\mathrm{d}t \cdot N_f$, normalized to n_0^i at the beginning of the process, depends on the ratio τ^i/τ^d, where n_0^i is the initial concentration of the excited radiating centers. Figure 4.10 shows the set of curves for different photon absorption cross sections by the color centers. Here $n_0^i = n_0^c = 1 \times 10^{18}$ cm^{-3} and σ has been chosen in the range of the typical spin and parity allowed transitions 10^{-14}–10^{-18} cm^2.

For small absorption cross section there is no change in the number of photons detected by the photodetector. However, the photon losses rapidly increase with increasing absorption cross section in the range of 10^{-16} to 10^{-14} cm^2. It is obvious that this effect is maximal when τ^i and τ^c are of the same order of magnitude. The absorption of photons by color centers is proportional to both the absorption cross section and the color center concentration. In real conditions where there are in general different types of color centers, we will observe the superposition of their contributions according to formulas (4.1).

Thus, even in the absence of metastable color centers but at high concentration of shallow traps, short lifetime centers can lead to a decrease of the scintillation output under the conditions of relatively high-energy release by ionizing radiation in a crystal.

The influence of short-lifetime absorption on the scintillation yield for the detection of γ-quanta and electrons at a small dose rate is negligible. However, the effect becomes substantial for a high excitation rate, for example, in the case of an intense pulse of high-energy γ-quanta.

As an example let us consider the influence of transient absorption on the light yield of a lead tungstate crystal. Recently, besides slowly recovering

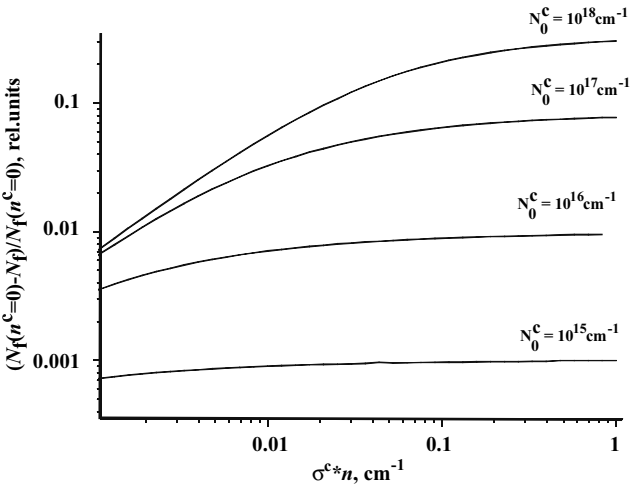

Fig. 4.11. Variation of the value $(N_f\ (n^c = 0) - N_f\ )\ /\ N_f(\ n^c = 0)$ as a function of $\sigma * n^c$ for concentrations of different color centers

color centers, a very fast decaying color center has been detected. This is a shallow electron type center, which forms a wide, short-wavelength, transient absorption band in the crystal with a maximum near 3.5 eV [79, 80] through the $^1A_1 \rightarrow {}^3T_1, {}^3T_2$ transitions in the unstable $WO_3{}^{2-}$ irregular tungstate center. Figure 4.11 shows the change as a function of $\sigma * n^c$ of the value $(N_f(n^c = 0) - N_f)/N_f(n^c = 0)$ where $N_f(\mathrm{n}^c = 0)$ is the number of photons to be detected in the case of the absence of color centers, for different color centers concentrations. This value is directly related to the deviation of the detector response from linearity. The decay time of scintillation τ^{I} is chosen to be 12 ns, a value of 60 ns is chosen for τ^c, and the value of the transient absorption $\sigma * n^c$ is estimated as $0.008\,\mathrm{cm}^{-1}$ from experimental data [79–81]. The typical concentration of oxygen vacancies, which produce these short-living color centers in lead tungstate, is about $10^{18}\,\mathrm{cm}^{-3}$.

Thus, the concentration of the color centers will be about 10^{17}–$10^{18}\,\mathrm{cm}^{-3}$ if we assume that 10–100% of point structure defects can trap charge carriers under ionizing radiation. One can see that the possible decrease of the light yield through transient absorption can be as large as 2–4%. On the one hand, this value may not seem very high. However, it can be critical for the practical use of scintillator (see, for instance, CT applications in Chap. 3).

Under very high irradiation doses the concentration of the color centers becomes high enough so that they start to actively interact with each other forming complex (new types) defects. Even radiation-hard crystal (such as for instance PWO) can become practically opaque to visible light. It is noteworthy that metastable defects after aggregation are transformed into very stable ones and that scintillation properties do not recover after several months

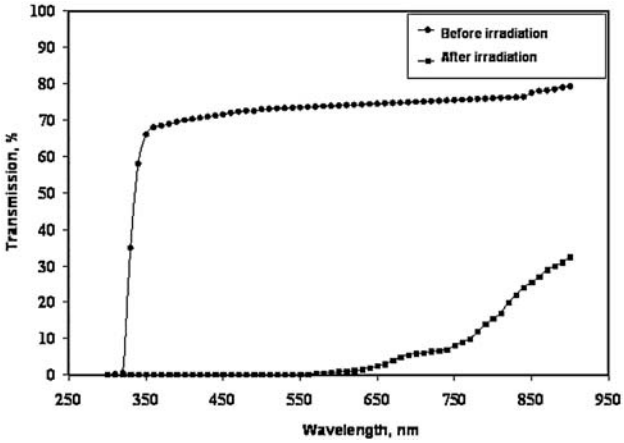

Fig. 4.12. Optical transmission spectra of the lead tungstate crystal with 0.2 mm width before and after irradiation by fast neutrons with 1.6×10^{20} neutrons cm^{-2} integral fluence. The measurement of the samples exposed to radiation was made a year and a half after irradiation

or even years of relaxation. Such situations arise when the concentration of radiation-induced damage reaches the same order of magnitude as regular ions of the lattice. Figure 4.12 shows the optical transmission spectrum of a 0.2-mm-thick lead tungstate plate before and after irradiation by fast neutrons with a fluence of 1.6×10^{20} neutrons cm^{-2}. An almost complete blackening of the material is observed. No scintillation can be seen anymore because the scintillation photons are immediately reabsorbed after their emission in the bulk of the material. A similar result was observed for BaF_2 scintillators but for much less heavy irradiation conditions [82]. After irradiation by a ^{60}Co source up to a dose of 1 Mrad crystals did not recover their transparency even after 260 days.

4.4.2.3 Impurity and Radiation Induced Color Centers

Considering the conditions of color centers formation and accumulation on the preexisting defects it is possible to divide them into two groups, namely, defects containing matrix base ions or vacancies and impurity-related defects. As the vacancy concentration corresponding to the crystal thermodynamic equilibrium at room temperature does not exceed $10^{-13}\,\mathrm{cm}^{-3}$ the concentration of color centers will be negligible for a visible change in crystal transparency even if all vacancy-type defects capture electrons or holes and create stable color centers. But real scintillators always contain different impurities potentially influencing the crystal transparency. Even the purest scintillation crystals contain impurities at the level of at least a few ppm. From the viewpoint of radiation coloring heterovalent impurities are the most harmful. In

such cases, the electrostatic balance in the crystal is restored by the formation of impurity-vacancy dipoles in which the vacancy compensates for the excess charge of the anionic or cationic impurity. A priori both types of impurities are harmful. The stabilization of an electron or a hole causes the stabilization of the center with opposite charge and, as a consequence, the creation of a stable color center.

The basic mechanisms of impurity-stimulated crystal coloring are described in [83–85]. Several studies were carried out in connection with the development of BaF_2 scintillator for the SSC project. In [54,55] many investigations are reviewed. To summarize it was shown that some cation impurities favor the accumulation of color centers, while some others slightly increase the radiation resistance of crystals.

From the alkaline-earth fluorides studies (CaF_2, SrF_2, BaF_2) the attention must be focused on two possible scenarios. The first one involves substitution impurity ions such as transition metal ions (partly filled 3d shell) and rare-earth ions (partly filled 4f shell). These types of impurities can easily change their valence state under irradiation and they have optical absorption bands in the visible and near ultraviolet spectrum. Even traces of such impurities can produce a significant radiation damage. The second scenario involves oxygen and hydrogen. These impurities can be introduced from the raw material and atmosphere during the growth process. The most likely mode of incorporation is OH^- ions substituting to fluorine. A low vacuum allows more moisture to enter into the crystal growth furnace. The scenario of radiation damage involves two process: the creation of F^- and $H^-$and the dissociation of OH^- radicals into O^- and interstitial $H_0{}^{\mathrm{i}}$ centers.

The optical absorption of an irradiated crystal before and after annealing is shown in Fig. 4.13. These data demonstrate the necessity to define special conditions to minimize the introduction of oxygen and hydrogen into the crystal. At some radiation dose the conversion of OH^- to UV active absorption centers is optimal. But annealing of UV absorption centers above a threshold temperature is possible as well as optical bleaching of these absorption bands.

According to [86] several metal impurities can also create additional complex color centers. They are produced according to the following chemical reactions:

$$\mathrm{M}^n + \mathrm{O}^{2-} + \mathrm{V}_\mathrm{a}^+ \rightarrow \mathrm{M}^{(n+1)+} + \mathrm{O}^{2-} + \mathrm{F} \ ,$$
$$\mathrm{M}^n + \mathrm{O}^{2-} + \mathrm{V}_\mathrm{a}^+ \rightarrow \mathrm{M}^{(n+1)+} + \mathrm{O}^{-} + \mathrm{F}^- \ ,$$

where M^{n+} is a metal ion, O is an oxygen ion, V_a is a vacancy of a fluorine ion and F is one "F" type color center.

O^{2-} is the most harmful ion for the radiation resistance of BaF_2. It is one of the three components of the complex color centers formation. OH^- is harmful through the production of oxygen and hydrogen centers.

It should be emphasized that the M^{n+} ion in the formula of complex color center must be a variable valence ion which can offer one or more free

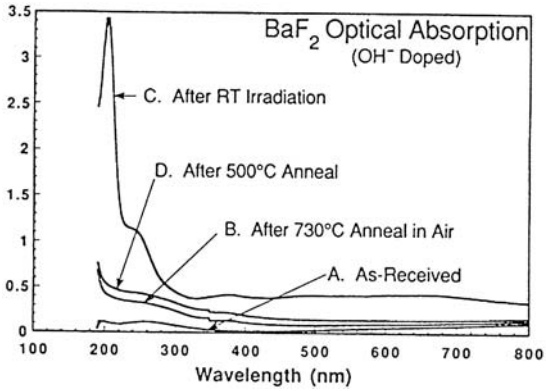

Fig. 4.13. Optical absorption as a function of (**B**) heat treatment, (**C**) irradiation (X-rays, 15 min), and (**D**) thermal annealing in argon [86]

electrons to form a complex color center during the irradiation. At the same time its valence state can affect the energy levels of simple color centers such as F and F^- centers and stabilize them at room temperature.

Similar effects are also typical for alkali-halide crystals where air components, oxygen above all, are the dominant impurities. The sources of such impurities are related to the insufficient purity of the raw material, the absorption of air components on the surface of raw material powder grains and the atmosphere of the single crystal growth furnace (see Chap. 6).

4.4.3 Radiation-stimulated Losses Scintillation Efficiency

Radiation damage studies in different scintillators showed that if scintillation losses are in most of the cases caused by the creation of color centers, they can in some cases be associated with a decrease of the luminescence yield. We will consider here some specific channels of the luminescence yield losses.

4.4.3.1 Excitation Reabsorption

The comparison of radiation-induced absorption with experimental data for Tl^+ excitation and emission bands [20, 72] reveals an overlapping of the hole-type center absorption maximum in Csl with that of the Tl ions excitation spectrum. The presence of stable hole centers causes a certain fraction of excitations to be trapped rather than transferred to TI^+ thereby causing nonradiative losses. As a result, the efficiency of energy transfer to luminescence centers drops, causing a decrease in the scintillation efficiency. The irradiation dose increases the concentration of hole centers and lowers the scintillation efficiency.

Thus, the radiation-induced color centers cause not only a loss in the light output of Csl(TI) crystals due to the transmission decrease (electron-type color centers), but they also influence the scintillation mechanism as a result of reabsorption of the TI^+ ion excitation (hole-type color centers).

At relatively small radiation doses the reabsorbing defects are related to the primary radiation point defects and color centers [72]. Sometimes such losses are not necessarily accompanied by the formation of visible color centers. In such cases the process is revealed by TSL measurement as it is related to the efficiency of energy storage in deep traps. In the crystal materials for which this efficiency is high can be used for information storage or dosimeters. A typical example in the sequence of alkali-halide crystals is given by CsI which is a scintillation matrix and by LiF for which the storage energy is so much larger that it has become the most widely used dosimeter material. Recent studies [87] of a multicomponent matrix of ABX_3 type (A—alkali metal, B—alkali-earth metal, X—halide ion) showed that special alloying makes it possible to suppress or, in contrast, increase the energy storage efficiency in a crystal (Table 4.3) Thus, the possibilities of radiation damage accumulation as a result of a modification of the structure cause the complete degradation of its scintillation features.

Table 4.3. Efficiency of luminescence and energy storage in $LiBaF_3$

Material	Core Valence	Self Trapped Exciton	Ce^{3+}	O^{2-}	Storage
$LiBaF_3$ pure	+++	+++	–	–	+
$LiBaF_3$(Ce)	++	++	+++	–	+
$LiBaF_3$(O)	++	++	–	++	++
$LiBaF_3$(Mg)	+–	–	–	–	+++
$LiBaF_3$(Mg,O)	+	+	–	++	+++
$LiBaF_3$(Ce,O)	++	++	++	+	+

At very high radiation dose absorption centers can be produced by rather complex radiation-induced defects. But in most of the cases the damage is caused by preexisting point defects and color centers.

4.4.3.2 Activator Ion Recharge

Another channel of luminescence efficiency losses is the reduction of activator ions concentration as a result of charge transfer process or solid state chemical reactions.

Since most of scintillators are activated crystals it is of importance to introduce activator ions in the correct valence state to guarantee the scintillation. This is often a difficult aspect of the crystal growth process (see Chap. 6).

Cerium-doped scintillation crystals suffer both optical absorption induced by ionizing radiation and scintillation mechanism damage. Depending on the conditions of synthesis the cerium ion is introduced in the crystals with a 2^+, 3^+, or 4^+ valence states, although the 3 valence state only gives rise to scintillation. The change in the balance between the different valence states under the action of irradiation (especially the recharge of Ce^{3+} ions to the Ce^{4+} state) reduces the concentration of luminescence centers and therefore the scintillation yield.

Let us consider the recharge of such impurity ions by irradiation. The "3+" cerium ion in oxide crystals and glasses are able to suppress slow recombination processes because of their large hole capture cross section. Furthermore, in some cases Ce^{3+} ions also favor the suppression of deep electron centers, thus causing a quick relaxation of some of the radiation-induced optical absorption. For this reason cerium is introduced in the fabrication of glasses when they have to be radiation hard. However, under irradiation of cerium-doped crystals, besides the well-known radiation-induced optical absorption bands, the effects of cerium ions recharge may be observed too. The radiation-induced variation in the concentration of three valence cerium ions means that the scintillation mechanism is modified. The irradiation of cerium-doped crystals may therefore reveal both changes in the optical properties of the crystals, i.e. formation of color centers, and variation in the luminescence efficiency through the modification of the initial valence state of the activator.

The radiation-induced spectra in undoped and Ce^{3+}-doped $YAlO_3$ crystals, as well as in $YAlO_3$:Ce_3^+ and $(Lu_{0.7}$-$Y_{0.3})AlO_3$:Ce_3^+ crystals, illustrate this situation.

In a nonactivated crystal the induced absorption extends over the whole visible range, its peak value reaching $400\,m^{-1}$ at maximum as seen in Fig. 4.14. For comparison even noncompensated lead tungstate crystals grown from cleaned raw material have an induced absorption coefficient two orders of magnitude smaller. The reason for such a big difference resides in a considerable shift from the optimal stoichiometry. The deficit of one of the cations causes a large increase of the anion (oxygen) vacancies contents in the crystal associated with a larger concentration of formation of color centers and to a worsening of the radiation hardness.

However, the induced absorption spectrum is deeply modified by cerium doping. The long-wavelength absorption bands are strongly suppressed. An intense peak near 270 nm is detected in the spectrum of activated crystals made by different methods. Figure 4.15 shows the induced absorption spectrum measured in $(Lu_{0.7}$–$Y_{0.3})AlO_3$:Ce^{3+} crystal grown by the Czochralski

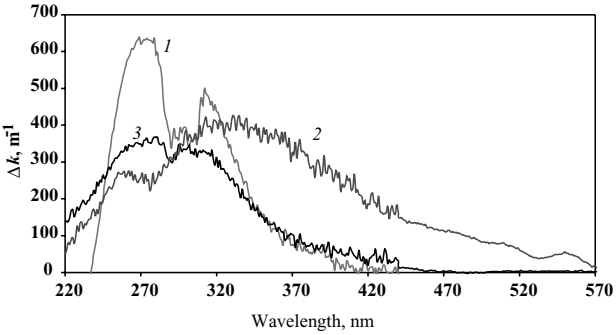

Fig. 4.14. Induced absorption spectra in $YAlO_3$ crystals grown by horizontal freeze method in vacuum: 1—Ce doped, 2—undoped crystal, 3—$YAlO_3$:Ce grown by the Czochralski method in Ar atmosphere. The conditions of irradiation are ^{60}Co (1.2 MeV), dose rate 7 kGy h^{-1}, accumulated dose 103 Gy, $T = 300$ K

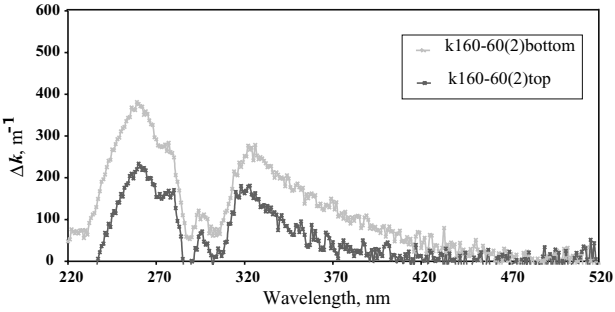

Fig. 4.15. Induced absorption spectra in $(Lu_{0.7}–Y_{0.3})AlO_3:Ce^{3+}$ crystals samples grown by the Czochralski method in inert gas atmosphere and cut out from the upper and lower part of a 180-mm long boule. Irradiation: ^{60}Co (1.2 MeV), dose rate 7 kGy h^{-1}, accumulated dose 103 Gy, $T = 300$ K

method in inert gas atmosphere. The measurements were carried out for the samples cut out from the upper and lower parts of a 180-mm long ingot. The induced absorption spectra are quite similar in shape and intensity for both yttrium mono-aluminate and solid solution of Lu–Y aluminate. It is quite evident that the defect formation process in both crystals is similar when using the same growth method, and, consequently, the approach for radiation hardness improvement for these crystals has to be the same.

In the induced absorption spectra of YAP and $(Lu_{0.7}–Y_{0.3})AlO_3$ crystals doped with Ce^{3+} ions there is a clear window near 300 nm. It is caused by the change in the Ce^{3+} ions excitation band intensity related to the change of the valence state of some of the activator ions. In other words, the radiation induces a charge transfer process and the transformation of the Ce^{3+} to Ce^{2+} valence state. Simple comparison between the initial and induced absorption

spectrum in this window indicates that at least 5% of Ce^{3+} ions are being recharged. Crystal annealing in oxygen atmosphere restores the initial spectra of activator absorption by a re-oxidation of the Ce^{2+} ions.

4.4.3.3 Radiation-Induced Chemical Reactions

While considering the effects induced by ionizing radiation it is necessary to distinguish one more aspect of it. It concerns radiation-induced chemical transformations, namely, the modifications in the impurity defects structure. The above-mentioned example of BaF_2 scintillators transparency loss is also typical here.

The absorption spectra from VUV to UV of BaF_2 before and after γ-irradiation are shown in Figs. 4.13 and 4.16.

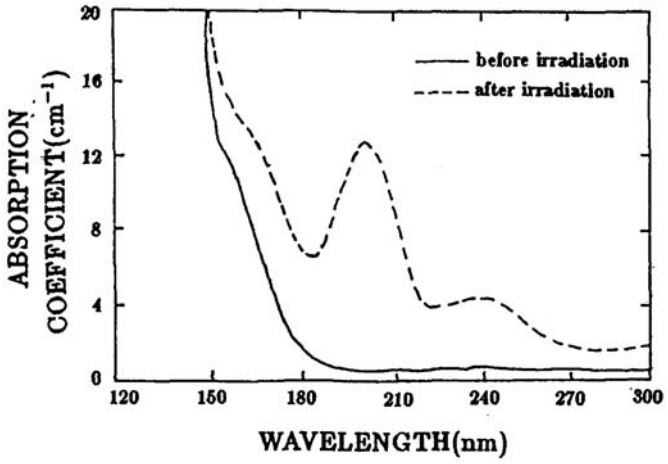

Fig. 4.16. Absorption spectra of hydrolyzed BaF_2, before and after irradiation [34]

A large radiation damage occurs in a treated sample, although no obvious absorption at 192 nm was found before irradiation. This result indicates that only a small amount of hydroxyl or oxygen impurities can lead to a serious radiation damage in BaF_2. Furthermore after irradiation a new peak of absorption at about 200 nm in the IR spectrum emerged, which is related to the H_S^- center.

The radiation-induced change was also observed in the EPR spectrum of hydrolyzed BaF_2 [34]. The spectrum was taken at room temperature with the magnetic field along the $\langle 100 \rangle$ crystal axis. Before irradiation no EPR signal was observed which means that the thermal treatment itself did not produce any modification of the EPR spectrum in BaF_2. After irradiation two groups of lines appeared separated by about 54 mT and symmetrically

placed around $g = 2$. It was concluded that this EPR signal is due to an interstitial atomic hydrogen $H_i{}^0$ in the center of an empty cube of fluoride. Moreover, the complex signal was observed in the central part ($g \sim 2$) of the same EPR spectrum. According to [86] one can state that the edge is probably due to the absorption of $O_S{}^{2-} - F^+$ related to the transition from the 2p level in oxygen to the 1s level of the F center. The EPR spectrum suggests that $H_i{}^0$ exists in treated BaF_2 after irradiation. H_i^0 centers come from the dissociation of OH^- through the radiolysis process,

$$OH^- \rightarrow O_S{}^- + H_i^0$$

The complex signal in the central part ($g \sim 2$) of the spectrum is partially due to $O_S{}^-$.

After irradiation two new absorption bands are observed in the UV range (Fig. 4.16). The H_S^- absorption peaks were also found in the UV and in the IR region. These results suggest that the absorption at 204 nm and ∼240 nm corresponds to H_S^- and O_S^- centers, respectively. The H_S^- center is probably produced by the process

$$H_i^0 + F \rightarrow H_S^-$$

where the center F is created independently under irradiation.

These examples cover only a small part of radiochemical reactions. In alkali-halide scintillators with activator-based luminescence there are also solid-state reactions involving thallium ions. The formation of complex color centers (such as for BaF_2) leads to both transparency loss and decrease in the activator luminescence efficiency. Due to some chemical reactions some centers are created which capture the electron excitations. On the other hand, these new centers can also produce additional luminescence.

Radiation damage of pure CsI scintillators is another interesting example which shows not only a drop of the scintillation yield under ionizing radiation but a complete redistribution of the scintillation kinetics. For this scintillator both the light output value of the fast UV scintillation (the emission peaks at about 300 nm) and the Fast/Total ratio (i.e. the ratio of the fast scintillation intensity to the total light output, i.e. the total amount of fast and slow components) are important parameters. An increase of the radiation-induced slow luminescence characterizes this material. Figure 4.17 shows that for increasing radiation dose the Fast/Total ratio decreases [20].

4.4.4 Approaches to Radiation Hardness Improvement

There are plenty of publications describing the radiation damage effects in many scintillators. However, there are a few descriptions of the methods of improving the radiation hardness of materials and there are no practical recommendations on the production technology of radiation hard scintillators. Primarily, they include (i) preventing radiation coloring in order to maintain the transparency of the scintillator at the emission wavelength; (ii) providing

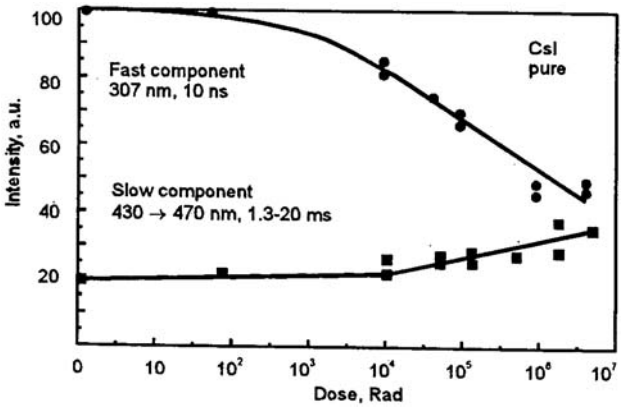

Fig. 4.17. Dose dependence of fast and slow emission components for nominally pure CsI scintillators

a good stability of the activator's state; (iii) suppressing parasitic luminescence; (iiii) minimizing losses at the energy transfer stage, etc.

This is generally considered as being part of the "know-how" of the crystal producers. However, it is very instructive to consider some general engineering approaches to produce radiation hard scintillators. These approaches are based on crystal annealing for the suppression of radiation defects; optical bleaching, i.e. the process of optically stimulated color centers annihilation; specific doping; etc.

Among the different methods of simultaneously suppressing the two radiation damage mechanisms (production of absorbing color centers and decrease of the scintillation efficiency) the use of specific doping is the most effective and widely applied. Certainly the first step is to try to produce crystals with the best intrinsic quality by the use of the highest purity raw materials and by reducing as much as possible the concentration of initial defects. But there is a technological and economic limit to this approach above which compensation of preexisting defects by specific impurities can be successfully used [88].

At the crystal growth of complex oxide compounds for instance, there is a progressive deviation from stoichiometry in the melt and in the grown crystal due to the different vapor pressures of the components of the melt. This leads to the creation of cation vacancies V_c and, as a consequence, to the production of charge-compensating anionic oxygen vacancies V_0 and associated defects of the same type. There is therefore a need to compensate the loss of cations and to simultaneously suppress the increase in the concentration of oxygen vacancies. This can be achieved by additional doping with an impurity ion of $(n+1)$ stable valence state, where n is the valence of the evaporating cation, and with an ionic radius as close as possible as the one of this cation in order to be easily localized in the same oxygen polyhedron. Besides, its segregation coefficient in the crystal growth process should be as close as possible to

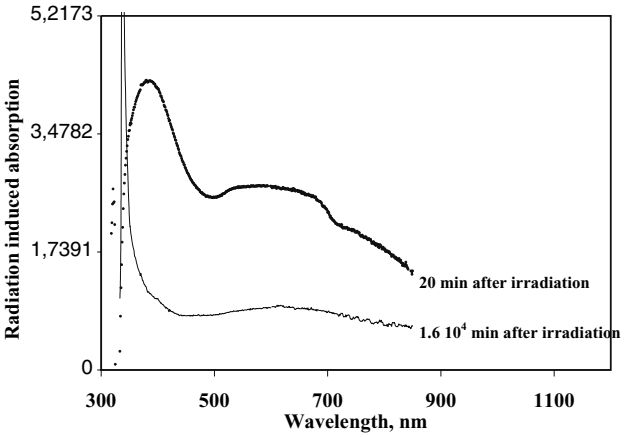

Fig. 4.18. Induced absorption spectra in a nonactivated lead tungstate crystal, measured 20 and 1.6×10^4 min after irradiation, radiation source is ^{60}Co, the dose rate is 10^4 rad h^{-1}, the irradiation time is 20 min, $T = 300$ K

one to allow for a homogeneous distribution. Such ions decrease the total amount of cationic vacancies in the crystal and bring an additional positive uncompensated charge which prevents the emergence of the V_0 vacancies.

Considering the PWO scintillator there is a dominating lead leakage from the melt during the growth leading to the formation of cationic vacancies V_c in the localization of the lead ion in the crystal lattice. A trivalent yttrium ion localized in the lead ion position meets all the above-mentioned requirements. As a result the concentration of cationic vacancies is strongly reduced and, consequently, the creation of anionic vacancies is also suppressed which significantly increases the radiation hardness of the crystal.

As is shown in Fig. 4.18 an undoped PWO crystal shows a dramatic deterioration of its optical transmission in the visible region under ionizing radiation. Crystal doping with yttrium with a concentration of approximately 100 ppm leads to a reduction of the absorption over the whole spectral range by an order of magnitude at least. A more detailed description of induced absorption spectrum and compensation mechanisms is presented in [23]. The same positive effect can be observed in the $PbWO_4$ crystals doped with trivalent La, Gd, and Lu ions. On the other hand, doping with heterovalent rare-earth ions such as Yb and Eu increases the induced absorption up to 200 m^{-1} [90].

Figure 4.19 shows the change of induced absorption at $\lambda = 420$ nm in the $PbWO_4$ crystals doped with different impurities depending on the accumulated dose of ^{60}Co γ-rays (1.23 MeV). For the accumulated doses of 10^4, 10^5, 10^6, 10^7, 10^8 rad, the dose rates were 10^4, 10^5, 3.3×10^5, 4.55×10^5, 10^6 rad h^{-1}, respectively. Crystals with a small number of vacancies because of La (Y-type ion) ion doping are characterized by an independence of the induced absorption with the dose rate up to 10^5 rad h^{-1}. It means that in

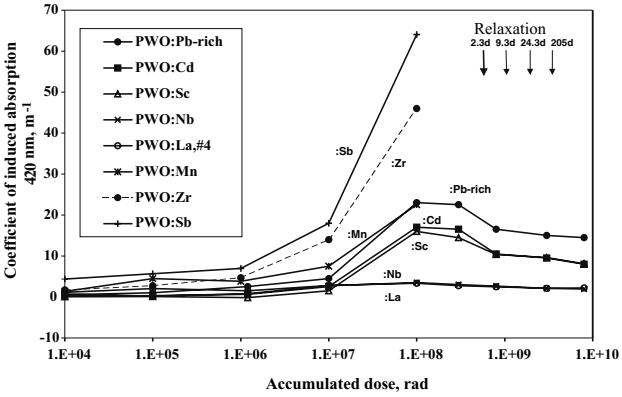

Fig. 4.19. Changes of induced absorption at $\lambda = 420\,\text{nm}$ in PWO crystals, activated with different impurities depending on the accumulated dose when irradiated by ^{60}Co (1.2 MeV), $T = 300\,\text{K}$ [95]

crystals with a small number of rechargeable centers, relatively small dose rates can cause the saturation of formation of electron and hole centers. On the other hand, for crystals doped with Sb and Zr ions a continuous increase of the induced absorption is observed that is obviously the consequence of a considerable rechargeable damage concentration with slow relaxation.

As the dose rate increases above 10^5 rad h^{-1} an additional increase of the induced absorption at $\lambda = 420\,\text{nm}$ takes place which grows with the dose rates. It is due to the fact that the first cause of the lead tungstate crystal matrix damage is the formation of a Frenkel pair. The signature of the Frenkel-type defect in lead tungstate is an absorption band near 350 nm. Under irradiation two electrons are captured by the Frenkel defect and form a deep electronic center [23,98]. This capture produces an annealing of the 350 nm band with a transfer to another band at 410 nm.

Depending on the concentration of the doping the induced absorption spectrum can be significantly modified because of the relative action of different color centers suppression mechanisms. For a concentration of 20–30 ppm La in the crystal, i.e. in the case when only a fraction of the vacancies is compensated by the trivalent impurities there is a strong suppression of the 620 nm band. But new bands at 520 and 470 nm as well as at 720 nm appear which have been masked in the absence of doping by the wide 620 nm band in the induced absorption spectrum. Figure 4.20 shows the spectrum of induced absorption for a $PbWO_4$:La crystal with a relatively small La concentration. At higher trivalent activator concentration there is a further decrease of all the color centers absorption bands. It is clearly shown in Fig. 4.21 for a crystal doped by 100 ppm Y^{3+} ions for measurements 1,674, 27,010, 86,185, and 165,883 s after irradiation. For optimal doping conditions the induced absorption spectrum envelop remains practically the same due to the simultaneous

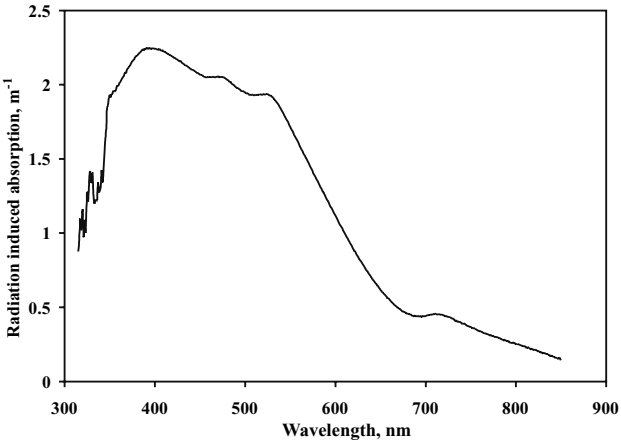

Fig. 4.20. Induced absorption spectrum of a $PbWO_4$:La crystal, the length is 23 cm, the La concentration is 20–30 ppm, the radiation source is ^{60}Co, the dose rate is 10^4 rad per hour, T = 300 K

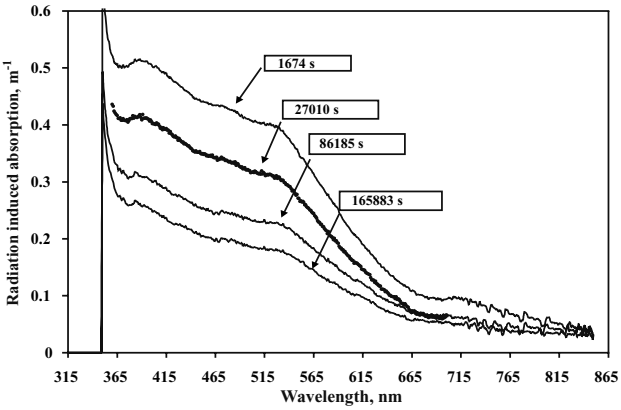

Fig. 4.21. Induced absorption spectra in the lead tungstate crystal, activated by yttrium ions with 80–100 ppm concentration, measured 1,674, 27,010, 86,185, and 165,883 s after irradiation, the source of radiation is ^{60}Co, the dose rate is 104 rad h^{-1}, the radiation time is 20 min, $T = 300$ K

suppression of all the bands and does not affect the light yield nonuniformity especially for long-size crystals. Such crystals with a low induced absorption are presently used for the production of the CMS calorimeter in CERN. Comparison of the spectra in Figs. 4.18, 4.20, and 4.21 shows that induced absorption spectra are different depending on the concentration of compensating impurity in the crystal. It means that damage and recovery kinetics of such crystals will also be different. It may have a negative impact on the energy resolution of calorimetric systems working in irradiation environment

with a complex time profile. That is why for precise electromagnetic calorimetry not only the value of the induced absorption at a given wavelength but also the reproducibility of the induced absorption spectrum from crystal to crystal in the scintillation spectral range has also to be specified.

The approach which works well for oxides is not as efficient for cross- luminescent fluoride crystals. An additional problem there is related to the possible UV absorption by optical transitions of the doping ion. Many rare- earth ions show in this region interconfiguration and charge transfer transitions. The method of radiation hardness improvement by doping with isovalent or aliovalent impurities has been investigated for the BaF_2 scintillator. The influence of alkali, alkali-earth, and rare-earth doping on the BaF_2 radiation damage has been systematically investigated. Doping ions have been divided into three groups: harmless elements, harmful elements, and useful elements. For example, La^{3+}, Lu^{3+}, and Y^{3+} are harmless for the radiation hardness of BaF_2 if the doping level is only of a few ppm. A strong absorption band was found at 1 ppm of Ce^{3+} or Pr^{3+} doping. The crystals doped with Eu^{3+}, Yb^{3+}, and Dy^{3+} show completely different results. These elements can eliminate color centers in the visible range and increase radiation hardness up to 1 Mrad irradiation while undoped crystals become brown at the same dose.

These studies were unfortunately stopped when the SSC project was closed down. The complete implementation of these ideas and methods for improving the radiation hardness in nonoxide crystals has been fulfilled for the CsI(Tl) and CsI(pure) scintillators.

The previous examples refer to the increase of the radiation hardness of undoped (self-activated) scintillators. However, as was already mentioned, most scintillators are activated crystals. The YAP:Ce scintillator is a characteristic example. The initial and gamma-radiation induced absorption spectra for different $YAlO_3$ crystals are shown in Fig. 4.22. The initial absorption center of the Ce^{3+}-doped crystal in the near UV range results from interconfiguration transitions from the ground state $4f^15d^0$ of the Ce^{3+} ion to a triplet level with the $5d^1$ configuration split by the crystal electrostatic field. Under irradiation the crystal shows an induced absorption at the level of several hundreds of inverse meters in the 220–500 nm spectral region. Doping the crystal with zirconium at the level of 100 ppm considerably improves these results.

The radiation-induced absorption in the emission range has been nearly completely suppressed in crystals doped with zirconium or annealed in hydrogen. Moreover, the recharging effect of Ce^{3+} also decreases and does not exceed 2%. In the $YAlO_3$ crystal growth process there is a dominant aluminum leakage from the melt [89]. The aluminum ion vacancies are compensated by zirconium ions localized in an oxygen octahedron. Zirconium ions also reduce the V_0 concentration in the crystal suppressing electron centers based on oxygen vacancies.

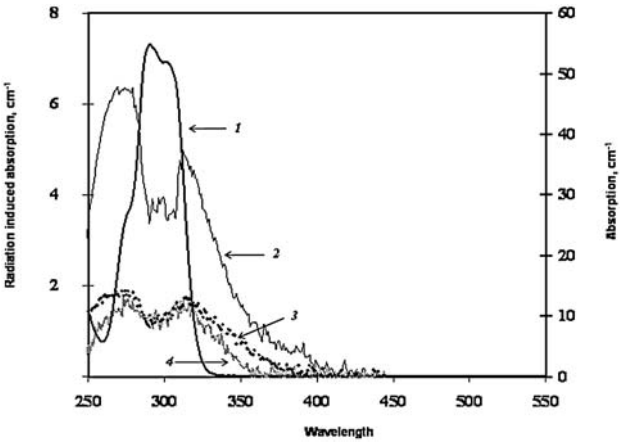

Fig. 4.22. Room temperature absorption spectra of the $YAlO_3$:Ce crystal: initial (*1*) after irradiation (*2*); induced absorption of a grown $YAlO_3$:Ce,Zr crystal (*3*) and the crystal grown and annealed in hydrogen (*4*); irradiation conditions: ^{60}Co (1.2 MeV), dose rate 7 kGy h^{-1}, accumulated dose 90 Gy

This approach is less suitable for complex oxides where one cation is localized in sites with several coordinations, for example, in crystals of $Y_3A_{15}O_{12}$, $Lu_3A_{15}O_{12}$ of the garnet structure, where aluminum ions are localized in octahedral and tetrahedral coordinations. The Zr ion is not really effective as it will go preferentially in octahedral coordination sites and leave uncompensated cation vacancies in tetrahedral sites. In this case co-doping by two impurity ions is required, one for each coordination site.

In conclusion it must be noticed that in spite of a longstanding research and development for radiation hard scintillators, no universal approach to suppress radiation damage has been found, if it exists at all.

Different approaches have been used for different materials. Figure 4.23 shows the level of radiation hardness for CsI(Tl) at the beginning (before intensive R&D effort) and at the end of the 1990s [91]. The possibility of radiation hardness improvement has allowed this crystal to be used not only for barrels but also for the end caps calorimeters where the radiation levels are generally one order of magnitude higher. The example demonstrates that the potential for radiation hardness improvement has not been exhausted even for thoroughly studied materials.

However, all the above-mentioned examples illustrate the basic mechanisms of radiation damage and the different methods which are applied to improve radiation hardness of scintillators. One may confidently say that the potential to produce more radiation hard scintillators is far from being exhausted.

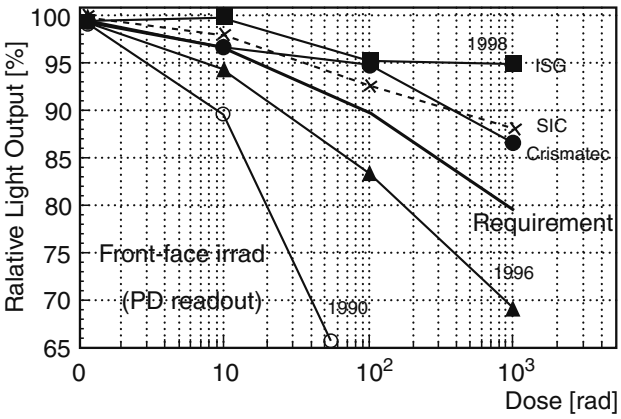

Fig. 4.23. CsI(Tl) scintillator. Radiation damage improvement during the last decade

4.5 Recovery of the Radiation-Induced Absorption

In many cases the radiation damage process is balanced by a spontaneous recovery of the crystal optical and luminescence parameters. This recovery occurs during irradiation and continues after irradiation is stopped. Such a phenomenon is typical both for halide and for oxide scintillators. The majority of radiation induced centers are not stable in time and their relaxation during the aging is the reason for the scintillation performance recovery. Moreover, point structure defects such as vacancies are generally not stable in the crystal at room temperature as they tend to sink to the dislocations or to the free surfaces. Therefore the recovery of the crystal structure also leads to the radiation damage recovery however in a longer time scale.

The recovery rate can also be accelerated by ionization of color centers by optical photons or by heating up the crystal up to a temperature where thermo-ionization of the deep electron and hole centers becomes possible. A well-known example of enforced recovery is the so-called optical bleaching of damaged materials: in a short time the initial spectral properties of the crystal are recovered by light illumination at a proper wavelength of the bulk material.

Most of the scintillation crystals are installed in complex experiments for a long operational time, and in a strong radiation environment, which makes enforced recovery difficult for technical reasons. Heating the detector is very often practically impossible. In real situations an acceptable radiation hardness behavior can be reached by tuning some of the crystal parameters in order to match the radiation exposure time profile to the damage and recovery kinetics of the crystal. For instance, a year cycle of the LHC accelerator will consist of three 60 days operation periods with high radiation levels, interleaved with 14 days stop intervals, where no radiation will be applied to

the experiments. After these three cycles there is a longer stop of the accelerator for about 150 days. During each of the 60 days periods the radiation level will follow the cycle of the accelerator beam intensity profile, with a continuous decrease of the collision rate during the runs, followed by machine refills. In spite of a precise monitoring system to correct for the crystal optical parameters changes, it is important to tune the crystal damage building and recovery kinetics to damp as much as possible the radiation exposure variations.

In the radiation environment of modern particle physics experiments the creation of new defects due to inelastic scattering of damaging particles is negligible. The radiation damage in the crystals in a relatively short time scale is therefore only the result of a charge-state change of preexisting point structure defects, which produce color centers. As a consequence the recovery process is driven by the relaxation of electronic states of these defects. As an example the model of the transmission radiation damage and recovery in lead tungstate crystals was proposed in [92]. It has been used for the optimization of the crystal technology development for the particular radiation environment of the CMS experiment at LHC. It is shown that the PWO transmission damage reaches a saturation level, which is dose-rate-dependent up to the point where the rate of trapping of the charge carriers induced by radiation is exactly balanced with the rate of spontaneous relaxation at this working temperature. In the case of a random distribution of the defects of type i in the crystal and in the absence of interaction between them the radiation damage will reach a saturation level after a certain time which is determined by the concentration of preexisting defects. The amount of damaged centers of type i is described by the following differential equation:

$$\frac{\mathrm{d}N_i}{\mathrm{d}t} = -\omega_i N_i + \frac{S}{d_i}(N_i^* - N_i) \,, \tag{4.2}$$

where N_i is the number of damaged centers of type i at time t, ω_i is the recovery rate of damaged centers of type i, S is the dose rate, N_i^* is the number of preexisting defects of type i, and d_i is the damage constant of the mentioned centers, which depends on the capture cross section of free carriers by the centers of type i. The induced absorption coefficient k produced by irradiation is proportional to the concentration of absorbing centers N through $k = \sigma N$, where σ is the cross section of the absorbing center. The solution of (4.2) can been given in terms of induced absorption:

$$k = k_\mathrm{sat} \frac{S}{S + \omega d} \left\{ 1 - \exp\left[-\left(\omega + \frac{S}{d} \right) t \right] \right\} \,, \tag{4.3}$$

where $k_\mathrm{sat} = N^* \sigma$ is the saturated induced absorption coefficient when all centers are damaged. The recovery of the transmission after the end of the irradiation at time t_0 is described by the following equation:

$$k = k_\mathrm{sat} \frac{S}{S + \omega d} \left\{ 1 - \exp\left[-\left(\omega + \frac{S}{d} \right) t_0 \right] \right\} \exp(-\omega(t - t_0)) \,. \tag{4.4}$$

Further investigations of short-term transient absorption, as well as the detection of photoionization processes involving electron centers, allowed us to develop a more adequate model of the radiation-induced absorption and of its recovery in lead tungstate crystals. A detailed description of electron and hole centers is given in Sect. 4.2 and [23, 98]. The defect energy level diagram in the forbidden band of a PWO crystal is shown in Fig. 4.24. In practice the electron centers created by irradiation in doped and undoped lead tungstate crystals can be divided into three groups. The first group consists of polaronic WO_4^{3-} centers, distorted regular centers WO_4^{2-}, and WO_4^{3-}-RE (where RE is a rare-earth cation). These centers are rather shallow, decay through the conduction band, and contribute to the scintillation mechanism. They can create a transient absorption band near the transmission band edge but it is not easy to distinguish their contribution from the background of fundamental absorption.

The second group is formed by different irregular WO_3^{2-} centers and more complex defects related to them. They have an average lifetime in the crystal

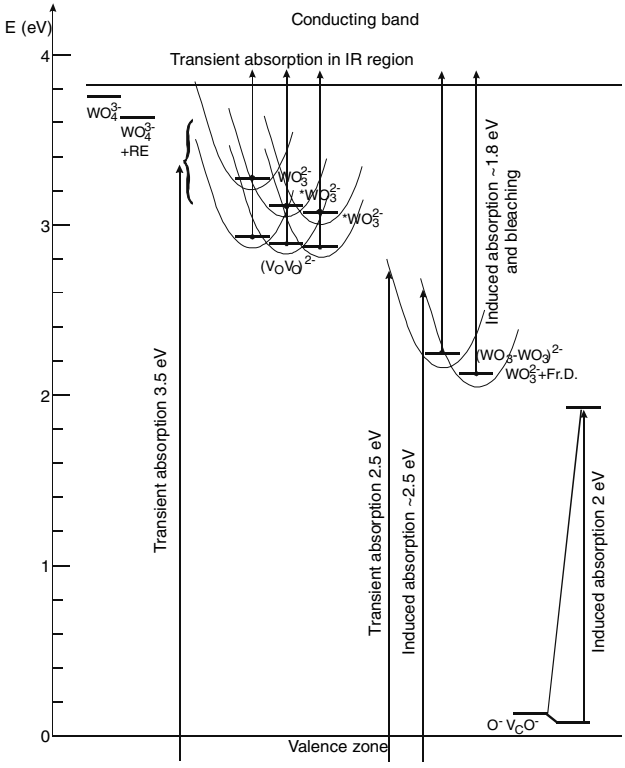

Fig. 4.24. The energy level diagram of electron- and hole-type centers in the forbidden band of PWO crystals

of about 10^{-6} s or even less and are quickly annihilated through thermoactivation at room temperature. In contrast to the centers of the first group, these irregular electron centers are either activated through a neighbor luminescence center WO_3, or their released electrons are captured by deeper traps such as MoO_4^{2-}. The ionization of these centers seems to be responsible for the transient absorption in the IR region [98]. The Pb^{1+}-V_0 center (where V_0 is an oxygen vacancy) contributes also to the IR transient absorption in the spectral region below 1,000 nm. Moreover, this group of defects is likely to form a wide, short-wavelength, transient absorption band in the crystal with a maximum near 3.5 eV.

The last group consists of associates of a dimer of $(WO_3–WO_3)^{2-}$ centers having captured two electrons and the Frenkel defect associated with $(WO_3)^{2-}$, which can also capture two electrons. The ionization of these deeper electron centers can also be observed through the bleaching by long-wavelength light [93] in the region of 1.8 eV ($\lambda \geq 700$ nm). The calculated annihilation rate of the deep associative center is in good agreement with experimental data [93–95] where a fast optical transmission recovery component has been detected. In contrast, the decay time of the electron center based on the Frenkel defect is much slower than the recovery time reported in [96]. In fact, slowly decaying induced absorption bands appear in lead tungstate crystals due to charge intracenter transitions of the Frenkel defect and di-hole centers. When crystals are doped with Latype trivalent ions the centers of the second and third groups are strongly suppressed. Figures 4.18, 4.20, and 4.21 show how the induced absorption spectra are modified from undoped to doped crystals. Depending on the crystal growth conditions and doping concentration at least five bands can be seen, peaked near 350–400, 470, 520, 620, and 720 nm. Following the description of the defects the transition between the ground and first excited state of the $O^-V_cO^-$ center is responsible for the 620 nm absorption band. The 720 nm band is due to the $(WO_3–WO_3)^{2-}$ center and the short-wavelength (350–400 nm) radiation-induced absorption band is caused by the recharge of the $(WO_3)^{2-}$-Frenkel defect center as mentioned above. The origin of the 470 and 520 nm bands is still debated [23]. Following a simple model of the thermo-activation and thermo-luminescence (TSL) data of electronic centers [97], one can estimate the spontaneous recovery time constants at room temperature of the $(WO_3–WO_3)^{2-}$ center and $(WO_3)^{2-}$-Frenkel defects to be 480 s and 10^4 s, respectively. Both absorption recovery constants can be observed in undoped crystals but their contribution in La(Y)-doped crystals is negligible. Figures 4.25a and 4.25b show the induced absorption recovery kinetics of undoped crystals at 400 nm (decay of electronic centers) and 600 nm (decay of hole centers). The kinetics curves are fitted with an exponential assuming that all centers decay through thermo-activation. The recovery kinetics is well described by two exponentials with 1,760 s (0.5 h) and 272,000 s (75 h) decay times. If the fast component is likely to be due to the decay of the $(WO_3–WO_3)^{2-}$ center, the longest one

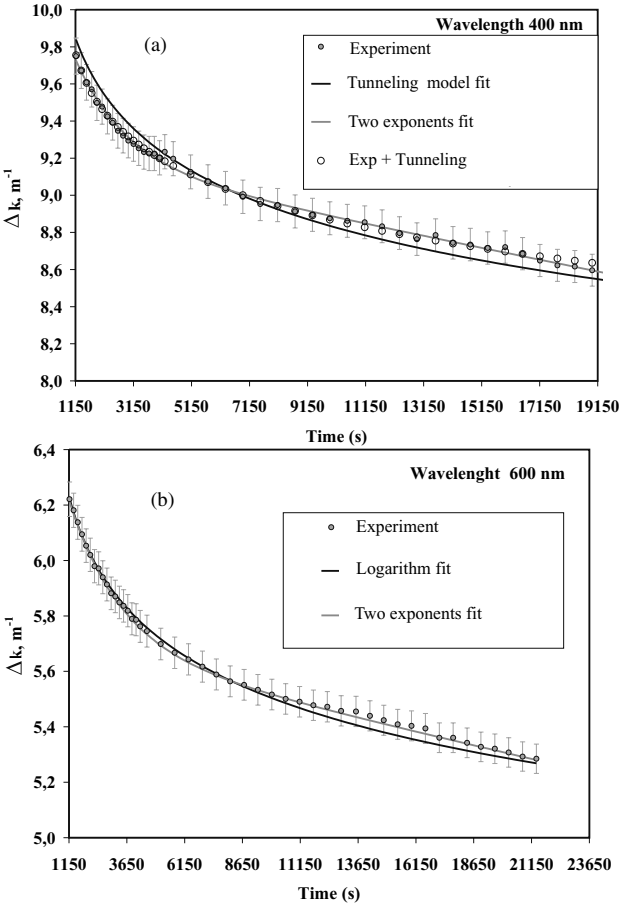

Fig. 4.25. Room temperature induced absorption recovery kinetics at 400 (**a**) and 600 (**b**) nm in an undoped lead tungstate crystal and their fits with (4.4) and (4.6)

cannot be attributed to the thermal decay. It seems that the only possibility of the electron/hole deep defects recombination is through the tunneling of the electron. Deep electron and hole centers do not have a correlated spatial distribution in the crystal and the tunneling rate approximation for a casual center distribution describes well the process of recovery in doped and undoped crystals.

PWO crystals present a unique situation where only two types of slowly decaying defects, the electronic Frenkel-type defect and the $O^-V_cO^-$-type centers, have a tunneling relaxation channel. Thus, the kinetics of defect concentration $n_t(t)$ decrease through tunneling of both electron$^-$ and hole-type centers is described by the same equation [97]:

$$n_t(t)/n_t(0) = 1/\left[1 + n_t(0)(\pi a^3/6)\ln^3 \nu t\right], \tag{4.5}$$

where $a = h/2\pi[2m(U_{\max} - E)]^{1/2}$, $n(0)$ is the initial concentration of electron defects, m is the mass of the electron, $U_{\max} - E$ is the difference between the potential barrier and the center energy, and ν is the hit frequency of the electron in the vibronic potential which is well approximated by the average frequency of the crystal phonon spectrum (500 cm^{-1}). In fact, the concentration of the defects at $t = 0$ is not defined. However, for numerical estimations, the concentration of the defects at very short time after irradiation (1 s for instance) can be chosen as the initial point.

The value $U_{\max} - E$ for a Frenkel defect associated with $(WO_3)^{2-}$ can be estimated taking into account the following argument. It is not less than 0.7 eV which is the thermo-activation energy of the center; however, it cannot be more than the ionization energy 1.8 eV of the center. In our approximation we used a value of 0.7 eV. As far as $U_{\max} - E$ and ν are defined, and $n(t)/n(0) = \Delta k(t)/\Delta k(0)$, where Δk is the induced absorption coefficient at the specified wavelength, the fit can give an estimation of the concentration of the defects in the crystal.

Thus the recovery which accounts for thermo-activation and tunneling effects is expressed by the equation

$$n(t)/n(0) = \left(\sum_i k_{i,\exp}(t) + k_{\mathrm{tun}}(t)\right)/k(0) \tag{4.6}$$

$$= \sum_i n_i(0)/n(0) \exp\left(-\frac{t}{\tau_i}\right) + n_t(0)/n(0)[1 + n_t(0)(\pi a^3/6)\ln^3 \nu t] \ ,$$

where $\Delta k_{i,exp}(0)$ is the induced absorption contribution of the exponential component of number i at $t = 0$, and $\Delta k_{\mathrm{tun}}(0)$ is the induced absorption contribution of centers recombining through tunneling at $t = 0$. Fit results are shown in Figs. 4.25 and 4.26 where recovery curves have been obtained from several standard CMS ECAL crystals after low-dose-rate (0.15 $\mathrm{Gy\,h}^{-1}$) irradiation. Data of the fit for different crystals are summarized in Table 4.4, where δt is the time between the end of irradiation and the beginning of measurements, λ is the wavelength of the measurement, and τ_{i} is the recovery constant of the exponential component number i. In these calculations we considered only one exponential component. The sum $\Delta k_{\exp}(0) + \Delta k_{\mathrm{tun}}(0) = \Delta k^{\mathrm{experimental}}$ is the value of the induced absorption measured immediately after the end of irradiation.

Undoped crystals show a fast recovery even 1,100 s after irradiation in the region of 400 nm (2.5 eV) where the $(WO_3{-}WO_3)^{2-}$ centers contribute. The decay time constant correlates well with the annihilation time of these traps determined through TSL measurements. The same fast component is observed at 600 nm. However, as seen from the fit, the majority of the electron and hole centers annihilate through tunneling. The best fit for 395 and 600 nm is found for $n(0) = 2.8 \times 10^{18}$ and 4.9×10^{18} cm^{-3}. The concentration of Pb^{2+} ions in the crystal is about $11 \times 10^{22}\,\mathrm{cm}^{-3}$, so the partial concentration

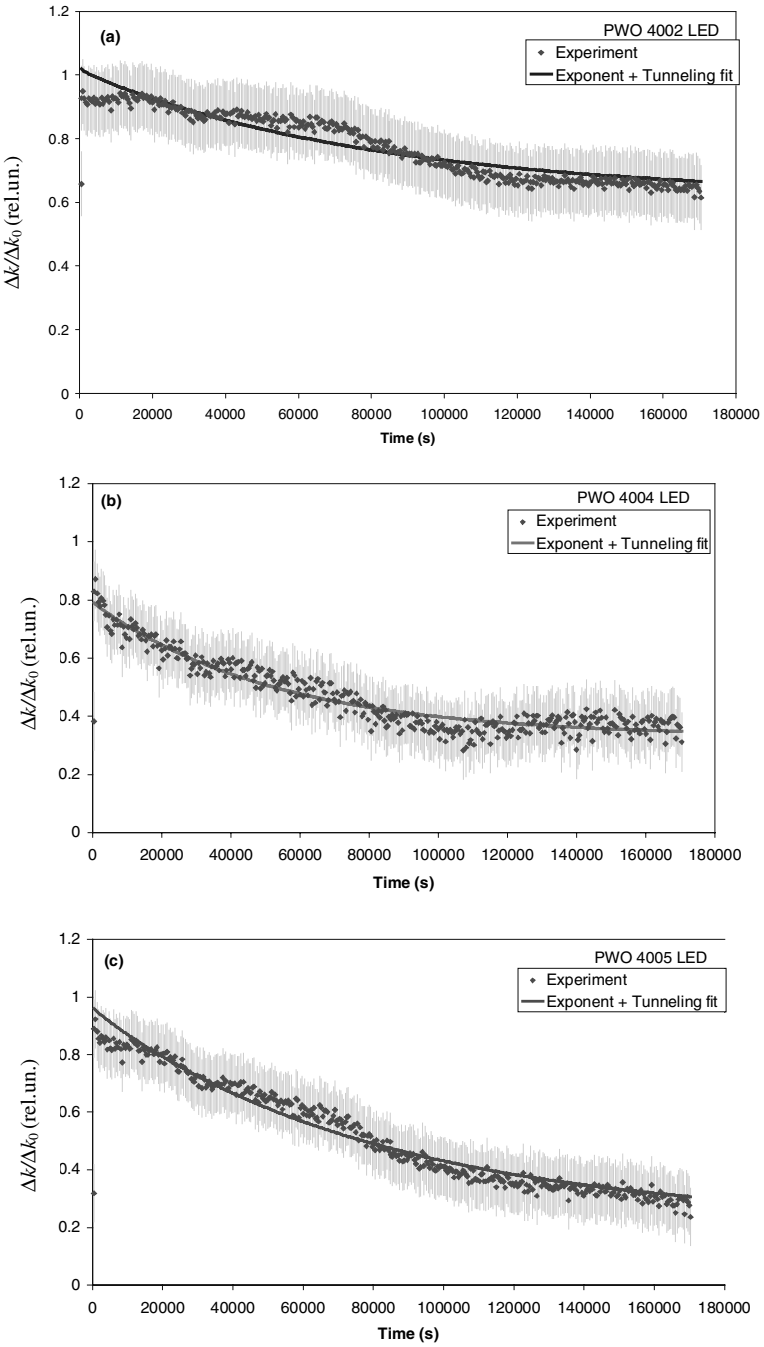

Fig. 4.26. Kinetics of the recovery at 470 nm of CMS ECAL crystals measured after 30 h irradiation with dose rate 0.15 Gy h^{-1} at room temperature. Small oscillations are due to residual temperature effects. Fit made by (4.6)

Table 4.4. Induced absorption recovery fit results of different PWO crystals

Sample	δt (s)	λ (nm)	τ_i (s)	$\Delta k_{exp}(0)$ (cm^{-1})	$n(0)$ (cm^{-3})	$\Delta k_{tun}(0)$ (cm^{-1})
PWO	1,100	395	448	1.1	2.8×10^{18}	20.4
		600	1,430	0.2	4.9×10^{18}	18.7
PWO:Y	1,100	400	77,000	0.75	4.1×10^{17}	0.48
		470	75,000	0.7	3.3×10^{17}	0.34
		600	69,000	0.36	2.7×10^{17}	0.16
		700	590	0.4		
#4002	100	470	81,500	0.068	1.7×10^{17}	0.120
#4004	100	470	53,170	0.051	6.7×10^{17}	0.053
#4005	100	470	80,000	0.103	5.6×10^{17}	0.038

of both types of defects is found to be of the order of tens of ppm. The value of the defect concentration is therefore in good agreement with the concentration value of the doping needed to suppress these defects in the crystal. When the crystal is doped with Y, there is a strong suppression of the $(WO_3–WO_3)^{2-}$ centers. No sign of a fast component with a recovery time less than 1,000 s is seen in doped crystals in the spectral region 400–600 nm. However, when the 620 nm induced absorption band is suppressed in the crystal, the detailed study of the recovery near 700 nm becomes possible. A recovery constant of 590 s is fitted in this spectral region strongly supporting the idea that this induced absorption band is also caused by the $(WO_3–WO_3)^{2-}$ centers as described above. Through the calculation of $\Delta k_{tun}(0)$ in Y(La) doped crystals, one can see that the amount of hole$^-$ and electronic-type centers is dramatically decreased. Moreover, the increase of $\Delta k_{tun}(0)$ corresponds to an increase of $n(0)$.

Nevertheless, an exponential component with a time constant in the range of 60,000–80,000 s is observed in the spectral region 400–600 nm in the recovery of all doped crystals. One could speculate that this slowly recovering center is created by the doping ion; however, as mentioned above, the Y(La) impurity ions do not create deep electron centers in the crystal. On the other hand, with the suppression of the 620 nm induced absorption band, the 470, 520 nm bands in the induced absorption become visible. It is therefore likely that the recovery of these absorption bands is characterized by this long time constant of 60,000–80,000 s. The data obtained and the modeling have shown that the suppression of the deep electronic and hole centers in the scintillation crystal is a good way to tune the recovery processes and to improve the calibration of the calorimeter on a long time scale.

References

1. Van Eijk CWC (2000) Inorganic scintillators for the next generation of neutron beam facilities. In: Mikhailin VV (Ed). Proc. of the Fifth Int. Conf. on Inorganic Scintillators and Their Applications, SCINT99. Moscow State University, Moscow, pp 22–32
2. Bisonnette JP, Munro P (1996) Evaluation of a high density scintillating glass for portal imaging, Med. Phys. 23: 401–406
3. Grynev BV, Seminozhenko VP (1993) Scintillation detectors for ruggedized applications. Osnova, Kharkov (in Russian)
4. Koepke BG, Anderson RH, Stokos RI (1976) Deformation in ceramics materials. In: Bradt RC (ed). Pergamon, New York–London, pp 497–513
5. Blasse G, Grabmaier BC (1994) Luminescence Materials. Springer, Berlin, pp 84–162
6. Koch A, Raven C (1997) Scintallators for high resolution x-ray imaging. In: Yin Zhiwen, Feng Xiqi, Li Peijun, Xue Zhilin (Eds). Proc. Int. Conf. on Inorganic Scintillators and Their Applications, SCINT'97. CAS, Shanghai Branch Press, Shanghai, pp 28–31
7. US Patents 4362946
8. US Patent 3960756
9. US Patent 4374749
10. US Patent 4375423
11. Gektin AV, Shiran NV, Pogorelova NV et al. (2002) Inorganic–organic rubbery scintillators. Nucl. Instrum. Methods Phys. Res. A 486: 191–195
12. Greskovich C, Duclos S (1997) Ceramic scintillators. Annu. Rev. Mater. Sci. 27: 69–88
13. US Patent 4747937.
14. Hirth JP, Lote J (1972) Theory of Dislocation. McGraw-Hill, New York, St. Louis, San Francisco, Toronto
15. Gektin AV, Krasovitskaya IM, Shiran NV (1984) Vacancy formation during plastic deformation of KCl crystals. Solid State Phys. 26: 2515–2517
16. Gektin AV, Serebryanny VYa, Shiran NV (1992) Point defect interaction and vacancy cluster formation in alkali halide crystals. Phys. Status Solidi a 134: 351–358
17. Ossipyan YA, Shmurak SZ (1981) Deformation luminescence and motion of charged dislocations in crystals. Defects in Insulation Crystals. Springer, Riga, Berlin, Heidelberg, pp 135–162
18. Bates CW Jr, Schneider I, Salau A et al. (1976) Strain-induced room temperature photoluminescence in CsI and CsI(Na). Solid State Commun 18: 101–103
19. Tyapunina NA, Tselebrovsky AN (1973) Vacancy concentration on plastically deformed NaCl type crystals. Crystallography 18: 649–650
20. Gektin AV, Shiran NV (1997) Scintillation losses in irradiated CsI-based scintallators. In: Yin Zhiwen, Feng Xiqi, Li Peijun, Xue Zhilin (Eds). Proc. Int. Conf. on Inorganic Scintillators and Their Applications, SCINT'97. CAS, Shanghai Branch Press, Shanghai, pp 115–120
21. Gavrilov VV, Gektin AV (1998) Deformation sensibilization of CsI based crystals. Solid State Phys. 30: 3163–3165
22. Bredikhin SI, Glushuk OA, Shmurak SZ (1982) Deformation sesibilisation of color centers in zinc selenide crystals. Solid State Phys. 24: 2249–2254 (in Russian: Fisika Tverdogo Tela)

23. Annenkov A, Korzhik M, Lecoq P (2002) Lead tungstate scintillation material. Nucl. Instrum. Methods Phys. Res. A 490: 30–50
24. Han Baoguo, Feng Xiqi, Hu Guangin et al. (1999) Annealing effects and radiation damage mechanisms of $PbWO_4$ single crystals. J. Appl. Phys. 86: 3571–3575
25. Böhm M, Henecker F, Hofstaetter A et al. (1998) Shallow electron traps in the scintillator material $PbWO_4$ to thermally stimulated luminescence In: Baccaro S, Borgia B, Dafinei I, Longo E (Eds). Tungstate Crystals. Proc. Int. Workshop on Tungstate Crystals, Rome, pp 139–146
26. Böhm M, Henecker F, Hofstaetter A et al. (1999) Electron traps in the scintillator material $PbWO_4$ and their correlation to the thermally stimulated luminescence. Radiat. Eff. Defects Solids 150: 413–417
27. Laguta VV, Rosa J, Zaritski MI et al. (1998) Polaronic WO_4^{3-} centers in $PbWO_4$ single crystals. J. Phys.: Condens. Matter 10: 7293–7302
28. Hofstaetter A, Alves H, Bohm M et al. (2000) Spectroscopic characterisation of defects in tungstate scintillators. In: Mikhailin VV (Ed). Proc. of the Fifth Int. Conf. on Inorganic Scintillators and Their Applications, SCINT99. Moscow State University, Moscow, pp 128–136
29. Hofstaetter A, Korzhik MV, Laguta VV et al. (2001) The role of the defect states in the creation of the intrinsic WO_3- centers in $PbWO_4$ by sub-band excitation. Radiat. Meas. 33: 533–536
30. Nikl M, Bonacek P, Nitsch K et al. (1997) Decay kinetics and thermoluminescence of $PbWO_4$: La^{3+}. Appl. Phys. Lett. 71: 3755–3757
31. Baccaro S, Bohacek P, Borgia B et al. (1997) Influence of La^{3+}-doping on radiation hardness and thermoluminescence characteristics of $PbWO_4$. Phys. Status Solidi a 160: R5–R6
32. Annenkov AN, Auffray E, Korzhik MV et al. (1998) On the origin of the transmission damage in lead tungstate crystals under irradiation. Phys. Status Solidi a 170: 47–62
33. Wang LM. Chen Y, Wu X (1994) Charge-state stability and optical transitions of oxygen impurities in barium fluoride crystal. Scintillator and Phospor Materials MRS Proc. 348: 399–406
34. Chen Lingyan, Du Jie, Wang Liming, Xiang Kaihua (1994) An investigation of radiation damage induced by hydroxyl and oxygen impurities in BaF_2 crystal. Scintillator and Phospor Materials MRS Proc. 348: 447–454
35. Pena JI (1988) Radiation effects in hydrolised CaF_2, SrF_2 and BaF_2. J. Phys. Chem. Solids 49: 273–278
36. Shamovsky LM, Glushkova AS (1963) Scintillators and scintillation materials. Kharkov 2: 5–2 (in Russian)
37. Nekrasov VN, Ivanovskt LE (1987) Melts 1: 82–85 (in Russian)
38. (a) Okada TJ (1981) Optical behavior of V centers in KI crystals at low temperatures. J. Phys. Soc. 50(2): 582–591
(b) Andrews L (1976) Optical spectra of the dibromide and diodide ions in the matrix-isolated $M^+Br_2^-$ and $M^+I_2^-$ species. Am. Chem. Soc. 98(7): 2152–2156
39. Rzepka E, Bernard M, Lefrant S (1998) V centers in irradiated alkali halide crystals. Nucl. Instrum. Methods Phys. Res. B 32: 235–237
40. Weber M., Lecoq P., Ruchti R., Woody C., Yen W., Zhu Ren-yuan, (Eds)(1994) Scintillator and Phospor Materials (MRS Proceeding, 348) 565pp

41. Korzhik MV, Pavlenko VB, Timoshenko TN et al. (1996) Spectroscopy and origin of radiation centers and scintillation in $PbWO_4$ single crystals. Phys Status Solidi a 154: 779–792
42. Annenkov AA, Fedorov AA, Galez Ph et al. (1996) The influence of additional doping on the spectroscopic and scintillation parameters of $PbWO_4$ crystals. Phys Status Solidi a 156: 493–503
43. Zang Y, Holzwarth NAW, Williams RT (1998) Electronic band structures of sheelite materials $CaMoO_4$, $CaWO_4$, $PbMoO_4$ and $PbWO_4$. Phys. Rev. 57: 12738–12750
44. Kubota S, Sakuragi S, Hashimoto S et al. (1988) A new scintillation material: Pure CsI with 10 ns decay time. Nucl. Instrum. Methods Phys. Res. A 268: 275–277
45. Gektin AV, Gorelov AI, Rykalin VI et al. (1990) CsI-based scintillators in γ-detection systems. Nucl. Instrum. Methods Phys. Res. A 294: 591–594
46. Nishimura H, Sakata S, Tsujimoto T, Nakayama M (1995) Origin of the 4.1 eV luminescence in pure CsI scintillator. Phys. Rev. B 51: 2167–2172
47. Gektin AV, Shiran NV, Charkina TA et al. (1992) radiation stability and afterglow problem for fast CsI-type Scintillators. Heavy Scintillators for Scientific and Industrial Applications. Frontieres, France, pp 493–498
48. Radzhbov A, Istomin A, Nepomnyashikh et al. (2005) Exciton interaction with impurity in barium fluoride crystal. Nucl. Instrum. Methods Phys. Res. A 537: 71–75
49. US Patent 5521387
50. Kostler W, Winnacker A, Grabmaier W (1993) Effect of Pr-codoping on the X-ray induced afterglow of $(Y,Gd)_2O_3$:Eu. J. Phys. Chem. Solids 56: 907–913
51. US Patent 5518658
52. Yoshida M, Nakagawa M, Fuji H et al. (1998) Application of Gd_2O_2S ceramic scintillator for X-ray solid state detector in X-ray CT. Japan. J. Appl. Phys. 27: L 1572–L1575
53. US Patent 5318722
54. Ren-ynan Zhu, Da-an Ma, Newman H (1994) Barium fluoride crystals for future hadron colliders. Scintillator and Phospor Materials. MRS Proc. 348: 91–98
55. Lecoq P (1994) Progress on scintillator research by the Crystal Clear Collaboration. Scintillator and Phospor Materials. MRS Proc. 348: 51–64
56. Baccaro S, Borgia B, Dafinei I, Longo E. (1998) Tungstate Crystals (Proc Int Workshop on Tungstate Crystals. Rome, Italy, 12–14 Oct. 1998), 393pp
57. BELLE Collaboration (1995),Technical Design Report, KEK Report 95-1.
58. BaBar Collaboration(1995), Technical Design Report, SLAC-R-95-457.
59. Kolontsova EV (1977) Radiation induced transformations in solids. In: Trefilov VI (Ed) Radiation Effects in Solids. Kiev, pp 107–112 (in Russian)
60. Kolontsova EV, Kulago EE (1972) Radiation effects in irradiated with neutrons single crystals of $LiNbO_3$, K_2SO_4, $NaNO_3$. Crystallography 17: 1197–1201 (in Russian)
61. Kolontsova EV, Kulago EE, Tomilin NA (1973) Radiation induced phase tension in a quartz. Crystallography 18: 1198–1201 (in Russian)
62. Mott NE, Gurney RW (1948) Electronic Process in Ionic Crystals. Oxford, p 304
63. Gektin AV, Serebrynny VYa, Shiran NV (1988) Color centers accumulation model for ionic crystals, Ukr. J. Phys. (in Russian) 33: 590–592

64. Aqullo-Lopez F, Jaque F (1973) Unified model for all stages of F-coloring of NaC. J. Phys. Chem. Solids 34: 1949–1960
65. (a) Hughes AE, Jain SC (1979) Metal colloids in ionic crystals. Adv. Phys. 28: 717–828
(b) Hughes AE (1983) Colloid formation in irradiated insulators. Radiat. Eff. 74: 57–76
66. Gektin AV, Charkina NA, Shiran NV et al. (1989) Optical absorption of colloidal particles in doped CsI crystals. Opt. Spectrosc. (Russian) 67(5)1989: 1075–1077
67. Kobayashi M, Sakuragi S (1987) Radiation damage of CsI(Tl) above 10^3 rad Nucl. Instrum. Methods 254a: 275–280
68. Renker D (1989) Technical report CERN N89-10 ECFA Study. Week Instrum. Technol. High-Luminosity Hadron Colliders 2: 601–610
69. Schotanus P, Kamermans R, Dorenbos P (1990) Scintillation characteristics of pure and Tl-doped CsI crystals. IEEE Trans. Nucl. Sci. 37: 177–182
70. Hitlin DD, Eigen G (1992) Radiation hardness study of CsI crystals. In: Heavy Scintillators for scientific and industrial applications. Frontieres, France, pp 467–478
71. Kobayshi M, Sakuragi S (1987) Radiation damage of CsI(Tl) crystals above 10^3 rad. Nucl. Instrum. Methods Phys. Res. A 254: 275–280
72. Gektin AV, Globus ME, Shepelev OA et al. (1997) Scintillation losses due to radiation damage in long CsI(Tl) crystals. Funct. Mater. 4: 544–547
73. Schulman J, Compton WD (1963) Color Centers in Solids. Pergamon, Oxford–London–New York–Paris, p 359
74. Hobbs LW, Hughes AE, Pooley D (1973) A study of interstitial clusters in irradiated alkali halides using direct electron microscopy. Proc. Roy. Soc. London A 332: 167–185
75. Jacobs G, Fiermans L, van de Wiele F (1961) Optical absorption of cesium halides with excess halogen. Physica 27: 144–148
76. Globus ME (1993) Spectrometric characteristics of ionizing radiation detectors based on BGO and CWO. Int. J. Radiat. Applic. Instrum. D 21: 131–133
77. Globus M, Grinyov B (1995) Calculations of scintillators for radiation detector systems: dependence of spectrometric characteristics on shape, size and reflector type. IEEE Trans. Nucl. Sci. 42: 357–360
78. Korjik M, Khrutchinsky A, Missevitch O et al. (2002) On the response linearity of scintillation detectors in irradiation environment. CMS IN 2002/056, p 9
79. Williams RT, Yochum HM, Ucer KB et al. (2000) Picosecond and nanosecond time-resolved study of luminescence and absorption of $CdWO_4$ and $PbWO_4$. In: Mikhailin VV (Ed). Proc. of the Fifth Int. Conf. on Inorganic Scintillators and Their Applications, SCINT99. Moscow State University, Moscow, pp 336–341
80. Millers D, Chernov S, Grigorieva L et al. (2000) Luminescence and transient absorption of doped PWO_4 scintillator crystals. In: Mikhailin VV (Ed). Proc. of the Fifth Int. Conf. on Inorganic Scintillators and Their Applications, SCINT99. Moscow State University, Moscow, pp 613–618
81. Grigorieva L. Private communication
82. Yin ZW (1994) Research and development works on BaF_2 crystals in Shanghai Institute of Ceramics. Proc. "Scintillator and Phospor Materials". MRS Proc. 348: 65–76

83. Ramos BS, Hernandes AJ, Muerietta SA et al. (1985) Model for F-center production in alkali halides doped with divalent cation impurities that change their valence state by irradiation Phys. Rev. B 31: 8164–8170
84. Annenkov AN, Auffray E, Borisevich A et al. (1999) Suppression of the radiation damage in lead tungstate scintillation crystal. Nucl. Instrum. Methods Phys. Res. A 426: 486–490
85. Haliburton LE, Edwards GJ (1994) Radiation damage mechanisms in scintillator materials: application to BaF_2 and CeF_3. Scintillator and Phosphor Materials. MRS Proc. 348: 423–434
86. Ren Saooxia, Chen Gang, Zhang Fengyin, Zheng Yanning (1994) The effect of impurities on the radiation damage of barium fluoride crystal. Scintillator and Phospor Materials. MRS Proc. 348: 435–440
87. Shiran N, Gektin AV, Ivanov N et al. (1999) The role of oxygen in energy transfer processes in $LiBaF_3$ scintillator. Mikhailin V., (Ed). Inorganic Scintillators and their Applications. Moscow pp. 230–235
88. Korzhik MV (2003) A general approach to increasing the radiation hardness of complex strucutre oxide scintillation crystals. Nucl. Instrum. Methods Phys. Res. A 500:116–120
89. Smirnova SA, Korzhik MV (1996) Growth of crystals of yttrium-aluminum perovskities with rare earth elements. In: Dorenbos P, van Eijk CWE (Eds). Proc. Int. Conf. on Inorganic Scintillators and Their Applications, SCINT'95. Delft University Press, The Netherlands, pp 495–497
90. Annennkov AN, Auffray E, Chipaux R et al. (1998) Systematic study of the short-term instability of $PbWO_4$ scintillator parameters under irradiation. Radiat. Meas. 29: 27–38
91. Gektin AV, (1999) Halide scintillators. Present status and prospects. In: Mikhailin VV (Ed). Proc. of the Fifth Int. Conf. on Inorganic Scintillators and Their Applications, SCINT99. Moscow State University, Moscow, pp 79–88
92. Annenkov AN, Auffray E, Fedorov A et al. (1997) Radiation damage kinetics in PWO crystals. CMS Note 1997/008, 9 pp.
93. Zhu RY, Ma DA, Newman HB et al. (1996) A study on the properties of lead tungstate crystals. Nucl. Instrum. Methods Phys. Res. A 376: 319–334
94. Nikl M, Bonacek P, Nitsch K et al. (1997) Decay kinetics and thermoluminescence of $PbWO_4$: La^{3+}. Appl. Phys. Lett. 71: 3755–3757
95. Kobayashi M, Usuki Y, Ishii M et al. (1998) Improvement in radiation hardness of $PbWO_4$ scintillating crystals by La-doping. Nucl. Instrum. Methods Phys. Res. A 404: 149–156
96. Nikl M, Nitsch K, Baccaro S et al. (1997) Radiation induced formation of color centers in $PbWO_4$ single crystals. J. Appl. Phys. 82: 5758–5762
97. Annenkov AN, Auffray E, Borisevich AE et al. (2002) On the mechanism of radiation damage in lead tungstate crystal optical transmission. Phys. Status Solidi A 191: 277–290
98. Korzhik MV (2003) Physics of scintillators on a base of oxide single crystals. Belarussian State University, Minsk